

Diffusive scattering of electrons by electron holes around injection fronts

I. Y. Vasko, O. V. Agapitov, F. S. Mozer, A. V. Artemyev, Vladimir Krasnoselskikh, J. W. Bonnell

▶ **To cite this version:**

I. Y. Vasko, O. V. Agapitov, F. S. Mozer, A. V. Artemyev, Vladimir Krasnoselskikh, et al.. Diffusive scattering of electrons by electron holes around injection fronts. Journal of Geophysical Research Space Physics, 2017, 122 (3), pp.3163-3182. 10.1002/2016JA023337 . insu-01520861

HAL Id: insu-01520861
https://insu.hal.science/insu-01520861

Submitted on 11 May 2017

HAL is a multi-disciplinary open access archive for the deposit and dissemination of scientific research documents, whether they are published or not. The documents may come from teaching and research institutions in France or abroad, or from public or private research centers.

L'archive ouverte pluridisciplinaire **HAL**, est destinée au dépôt et à la diffusion de documents scientifiques de niveau recherche, publiés ou non, émanant des établissements d'enseignement et de recherche français ou étrangers, des laboratoires publics ou privés.

AGU PUBLICATIONS

JGR

Journal of Geophysical Research: Space Physics

RESEARCH ARTICLE
10.1002/2016JA023337

Diffusive scattering of electrons by electron holes around injection fronts

I. Y. Vasko[1,2], O. V. Agapitov[1,3], F. S. Mozer[1], A. V. Artemyev[2,4], V. V. Krasnoselskikh[5], and J. W. Bonnell[1]

[1]Space Science Laboratory, University of California, Berkley, California, USA, [2]Space Research Institute of Russian Academy of Science, Moscow, Russia, [3]Astronomy and Space Physics Department, Taras Shevchenko National University of Kiev, Kiev, Ukraine, [4]Department of Earth, Planetary, and Space Sciences and Institute of Geophysics and Planetary Physics, University of California, Los Angeles, California, USA, [5]LPC2E/CNRS, University of Orleans, Orleans, France

Key Points:
- Electrostatic broadband turbulence around injection fronts in the outer radiation is due to electron phase space holes
- Electron holes drive efficient pitch angle and momentum scattering of gyroresonant electrons (typical energies are below a few keV)
- Bounce-averaged diffusion coefficients driven by electron holes for electrons below a few keV are comparable to those due to chorus and electron cyclotron harmonics

Correspondence to:
I. Y. Vasko,
vaskoiy@gmail.com

Citation:
Vasko, I. Y., O. V. Agapitov, F. S. Mozer, A. V. Artemyev, V. V. Krasnoselskikh, and J. W. Bonnell (2017), Diffusive scattering of electrons by electron holes around injection fronts, *J. Geophys. Res. Space Physics*, *122*, doi:10.1002/2016JA023337.

Received 15 AUG 2016
Accepted 12 FEB 2017
Accepted article online 20 FEB 2017

©2017. American Geophysical Union. All Rights Reserved.

Abstract Van Allen Probes have detected nonlinear electrostatic spikes around injection fronts in the outer radiation belt. These spikes include electron holes (EH), double layers, and more complicated solitary waves. We show that EHs can efficiently scatter electrons due to their substantial transverse electric fields. Although the electron scattering driven by EHs is diffusive, it cannot be evaluated via the standard quasi-linear theory. We derive analytical formulas describing local electron scattering by a single EH and verify them via test particle simulations. We show that the most efficiently scattered are gyroresonant electrons (crossing EH on a time scale comparable to the local electron gyroperiod). We compute bounce-averaged diffusion coefficients and demonstrate their dependence on the EH spatial distribution (latitudinal extent and spatial filling factor) and individual EH parameters (amplitude of electrostatic potential, velocity, and spatial scales). We show that EHs can drive pitch angle scattering of $\lesssim$5 keV electrons at rates $10^{-2} - 10^{-4}$ s^{-1} and, hence, can contribute to electron losses and conjugated diffuse aurora brightenings. The momentum and pitch angle scattering rates can be comparable, so that EHs can also provide efficient electron heating. The scattering rates driven by EHs at L shells $L \sim 5-8$ are comparable to those due to chorus waves and may exceed those due to electron cyclotron harmonics.

1. Introduction

Van Allen Probes detect intense broadband electrostatic wave activity below a few hundred hertz on the nightside in the outer radiation belt [*Mozer et al.*, 2014; *Malaspina et al.*, 2014]. This wave activity is observed over a wide magnetic local time (MLT) range (with the occurrence frequency peak at the premidnight sector) at L shells higher than $L \sim 4.5$ [*Malaspina et al.*, 2014]. *Malaspina et al.* [2015] have demonstrated a high correlation between observations of the broadband electrostatic wave activity and injection fronts. Multispacecraft observations have proved this wave activity to be continuously generated around injection fronts during their inward propagation [*Malaspina et al.*, 2015]. Observations of similar wave activity by Time History of Events and Macroscale Interactions during Substorms (THEMIS) spacecraft in the flow braking region, $L \sim 11$, supports this conclusion [*Deng et al.*, 2010; *Ergun et al.*, 2009, 2015].

High-cadence burst waveform data have demonstrated that the broadband electrostatic wave activity is due to nonlinear large-amplitude electrostatic spikes collectively referred to as time domain structures (TDS) and including electron holes, double layers, and sometimes more complicated solitary waves [*Mozer et al.*, 2013, 2015; *Malaspina et al.*, 2014, 2015]. TDS have typical electric field amplitudes of a few tens of mV/m and spatial scales of about a few kilometers and propagate with velocities of a few thousand km/s almost along the magnetic field lines [*Mozer et al.*, 2015]. Electron holes are characterized by a bipolar parallel electric field, a positive peak of the electrostatic potential, and a negligible net parallel potential drop. They also exhibit substantial transverse electric fields indicating their three-dimensional configuration with comparable parallel and transverse spatial scales [*Vasko et al.*, 2017]. On the contrary, double layers are largely one-dimensional with negligible transverse electric fields and almost unipolar parallel electric field [*Mozer et al.*, 2013; *Vasko et al.*, 2015a].

The role of TDS in the electron energization and loss in the outer radiation belt is being actively investigated. Similarly to oblique whistlers [*Cattell et al.*, 2008; *Kellogg et al.*, 2010; *Agapitov et al.*, 2014, 2015], TDS can trap

thermal electrons at the equator and transport them to higher latitudes resulting in electron energization [*Artemyev et al.*, 2014; *Vasko et al.*, 2016]. This nondiffusive process is able to promptly generate flux enhancements of up to hundred keV electrons [*Mozer et al.*, 2016a] for further acceleration by whistler waves [*Thorne*, 2010; *Mozer et al.*, 2014; *Ma et al.*, 2016]. In this paper we show that TDS can drive efficient diffusive scattering (in pitch angle and momentum) of ambient electrons (not trapped within TDS) with energies below a few keV. Therefore, in addition to whistler waves and electron cyclotron harmonics [*Thorne et al.*, 2010; *Ni et al.*, 2011a, 2011b; *Su et al.*, 2010], TDS can contribute to diffuse aurora precipitations [*Swift*, 1981; *Newell et al.*, 2009; *Ni et al.*, 2016].

The local scattering can be driven by double layers due to their net parallel potential drops, which result in parallel electron momentum variations. However, this scattering is largely canceled out after the bounce-averaging, since electrons bounce back and forth along about the same number of double layers distributed along the magnetic field lines. On the contrary, electron holes (EHs) can drive irreversible scattering due to their substantial transverse electric fields. In what follows, we consider the scattering driven by EHs.

EHs are in principle nonlinear plasma modes [*Gurevich*, 1968; *Schamel*, 1982]. The EH electrostatic field could be certainly expanded into the Fourier integral and would represent a packet of planar electrostatic waves with different wavenumbers propagating with the same phase velocity at different wave-normal angles. However, none of these waves is a linear plasma eigenmode. Therefore, the scattering driven by EHs cannot be evaluated via the standard quasi-linear theory [*Vedenov et al.*, 1961; *Vedenov*, 1963; *Drummond and Pines*, 1964; *Kennel and Engelmann*, 1966] widely used to evaluate the scattering driven by a turbulence of linear plasma modes in the outer radiation belt [*Kennel and Petschek*, 1966; *Lyons et al.*, 1972; *Shprits et al.*, 2008; *Glauert et al.*, 2014]. At the same time, the interaction of ambient electrons with EHs can be diffusive [*Chandrasekhar*, 1943], since under certain conditions (specified below) multiple interactions with different EHs result in small and uncorrelated pitch angle and momentum variations. The scattering rates driven by EHs can be inserted into the Fokker-Plank equation [*Albert and Young*, 2005; *Shprits et al.*, 2008; *Xiao et al.*, 2009, 2010] to describe the corresponding evolution of the electron phase space density.

In this paper we show that the local scattering by a single EH is most efficient for electrons crossing EH on a time scale comparable to the local electron gyroperiod, $|V_\parallel - V_\phi| \sim \omega_c d_\parallel$, where V_ϕ, $d_\parallel$ are the EH velocity and typical parallel scale, and ω_c and $V_\parallel$ denote local electron gyrofrequency and its parallel velocity. The physical mechanism of this scattering is deceleration (or acceleration) by the transverse electric field that is mostly along (or opposite to) the electron transverse velocity in the course of EH crossing. Formally speaking, this scattering is due to cyclotron resonances (of all orders) with planar electrostatic waves contributing to the Fourier expansion of the EH electrostatic field. We refer to these most efficiently scattered electrons as gyroresonant. Similarly to a resonance with a linear wave [*Shklyar and Matsumoto*, 2009; *Ukhorskiy and Sitnov*, 2013], the gyroresonance with EH has some width in the velocity space, $\omega_c d_\parallel(1-\delta_c) \lesssim |V_\parallel - V_\phi| \lesssim \omega_c d_\parallel(1+\delta_c)$, where parameter δ_c (smaller but of the order of 1) takes into account that electrons crossing EH on a time scale of about the electron gyroperiod are scattered efficiently.

The gyroresonance can generally overlap with the Landau resonance, $|V_\parallel - V_\phi| \lesssim \Delta V_L$, where $\Delta V_L = (2e\Phi_0/m_e)^{1/2}$ is the Landau resonance width depending on the amplitude Φ_0 of the EH electrostatic potential [*Shklyar and Matsumoto*, 2009]. The "overlapping" parameter $\Delta_{LC} = \omega_c d_\parallel / \Delta V_L$ determines whether the resonances overlap each other [*Zaslavskii and Chirikov*, 1971]. In the case of highly isolated resonances, $\Delta_{LC} \gg 1$, Landau resonant electrons are scattered inefficiently, while the scattering of gyroresonant electrons is diffusive and can be evaluated analytically. The regime of isolated resonances is generally realized for EHs in the outer radiation belt. In the case of substantially (or partially) overlapped resonances, $\Delta_{LC} \lesssim 1$, the scattering becomes more efficient, while our theoretical analysis provides, as we show, only lower estimates for the scattering rates. In this regime the scattering should be also nondiffusive, since electron trapping into the EH electrostatic potential may occur frequently. However, it is unlikely that this regime of scattering is realized in the space plasma, since in this regime EHs are unstable and decay rapidly [*Muschietti et al.*, 2000].

In this paper we derive analytical formulas for the local scattering rates driven by a single EH at some fixed latitude (assuming isolated resonances) and verify them using test particle simulations. Then, we compute bounce-averaged diffusion coefficients [*Lyons et al.*, 1972; *Glauert and Horne*, 2005] taking into account typical EH parameters, the EH spatial filling factor (number of EHs per unit volume), and latitudinal extent of the region, where EHs are concentrated. The typical EH parameters are adopted from our previous statistical study

of more than 100 EHs observed around one particular injection front [*Vasko et al.*, 2017]: most frequently, EH velocities are from 2000 to 7000 km/s, EH amplitudes are from 20 to 60 V, and EH parallel scales are from 0.3 to 1.3 km. The EH spatial filling factor is evaluated in this paper based on Van Allen Probes observations of one typical injection front. We compute and compare bounce-averaged diffusion coefficients assuming EHs concentrated below several maximum latitudes, since EHs are observed at all latitudes covered by Van Allen Probes, $|\lambda| \lesssim 18°$. We also compute diffusion coefficients at different L shells and compare them to those for chorus waves and electron cyclotron harmonics [*Ni et al.*, 2016].

The paper is organized as follows. In section 2 we evaluate the EH spatial filling factor. In section 3 we analyze the scattering driven by a single EH. In section 4 we describe computation of bounce-averaged diffusion coefficients and find out their scalings with the EH spatial filling factor and amplitude of EH electrostatic potential. In section 5 we adopt the evaluated EH spatial filling factor to demonstrate realistic pitch angle diffusion coefficients in dependence on EH parameters and L shell. In section 6 we discuss and summarize our results.

2. Observations: EH Spatial Filling Factor

We consider one typical injection observed by Van Allen Probes on 29 June 2013. We use data provided by the following instruments: Electric Field and Waves (EFW) instrument [*Wygant et al.*, 2013], Electric and Magnetic Field Instrument Suite and Integrated Science (EMFISIS) [*Kletzing et al.*, 2013], and Energetic Particle, Composition, and Thermal Plasma (ECT) instrument [*Spence et al.*, 2013]. The electric and magnetic fields are presented in the magnetic field-aligned coordinate system with the Z axis along the background magnetic field.

Figure 1c presents an injection identified by flux enhancements of about 10 keV electrons observed around 6:45 UT at $L \sim 5.9$, at latitude $\lambda \sim 13°$ and around local time 21.5 MLT. Figures 1a and 1b present spectra of electric and magnetic field fluctuations. There is no significant wave activity in frequency ranges corresponding to chorus waves (between one and one tenth of the electron gyrofrequency) and electron cyclotron harmonics (above the electron gyrofrequency). The most intense are electrostatic field fluctuations below a few hundred hertz accompanied with lower frequency magnetic field fluctuations corresponding likely to kinetic Alfven waves [*Chaston et al.*, 2014, 2015; *Moya et al.*, 2015]. Figure 1d provides about 10 min interval (6:42–6:55 UT) of measurements of the electric field averaged every 0.125 s over the frequency range [50, 300] Hz. The averaged electric field indicates three sequential bursts of the electrostatic wave activity at 6:43–6:46, 6:46–6:48:30, and 6:48:30–6:52 UT.

Figures 1a and 1d show that the broadband wave activity is observed around the injection front for about 10 min. The previous multispacecraft studies have shown that injection fronts observed in the outer radiation belt propagate inward with velocities of about 25–50 km/s [*Reeves et al.*, 1996; *Malaspina et al.*, 2015; *Liu et al.*, 2016]. Therefore, the region filled with the broadband wave activity has the radial spatial extent of about 3 R_E. The azimuthal (or MLT) extent of this region is likely of the same order [see, e.g., *Sergeev et al.*, 1996, 2012; *Nakamura et al.*, 2004].

The electric field measurements of EFW instrument in the burst mode regime (16,384 samples/s) are available for a limited number of 5 s time intervals. Figure 1e presents about 10 s interval around 6:45:40 UT of measurements of three electric field components in the burst mode regime. Figure 1f provides 1 s subinterval of the parallel electric field measurements. Figures 1e and 1f confirm that the broadband electrostatic wave activity is due to electrostatic spikes, i.e., TDS, with amplitudes up to 40 mV/m. Figure 1e shows that TDS are observed in groups with each group lasting for a few seconds and a time interval between two sequentially observed groups of about a few tenths of seconds. Figure 1f shows that within a group, there are more than 10 TDS every 100 ms, so that the typical time interval between two sequentially observed TDS is less than 10 ms.

Figure 1g provides an expanded view of one of TDS. The interferometry analysis of TDS observations by different EFW probes [*Mozer et al.*, 2013] shows that this TDS propagates with velocity of about 4200 km/s almost along the magnetic field lines (in the direction opposite to the background magnetic field, i.e., $V_\phi \sim -4200$ km/s). TDS has bipolar parallel and more or less unipolar transverse electric fields. The electrostatic potential computed as $\int E_\parallel V_\phi dt$ and presented in Figure 1g has a positive peak $\Phi_* \sim 15$ V and a negligible parallel potential drop. The positive peak of the electrostatic potential indicates that the observed TDS are three-dimensional EHs (for EH models see, e.g., *Schamel* [1982], *Jovanović et al.* [2002], and *Chen et al.* [2005]).

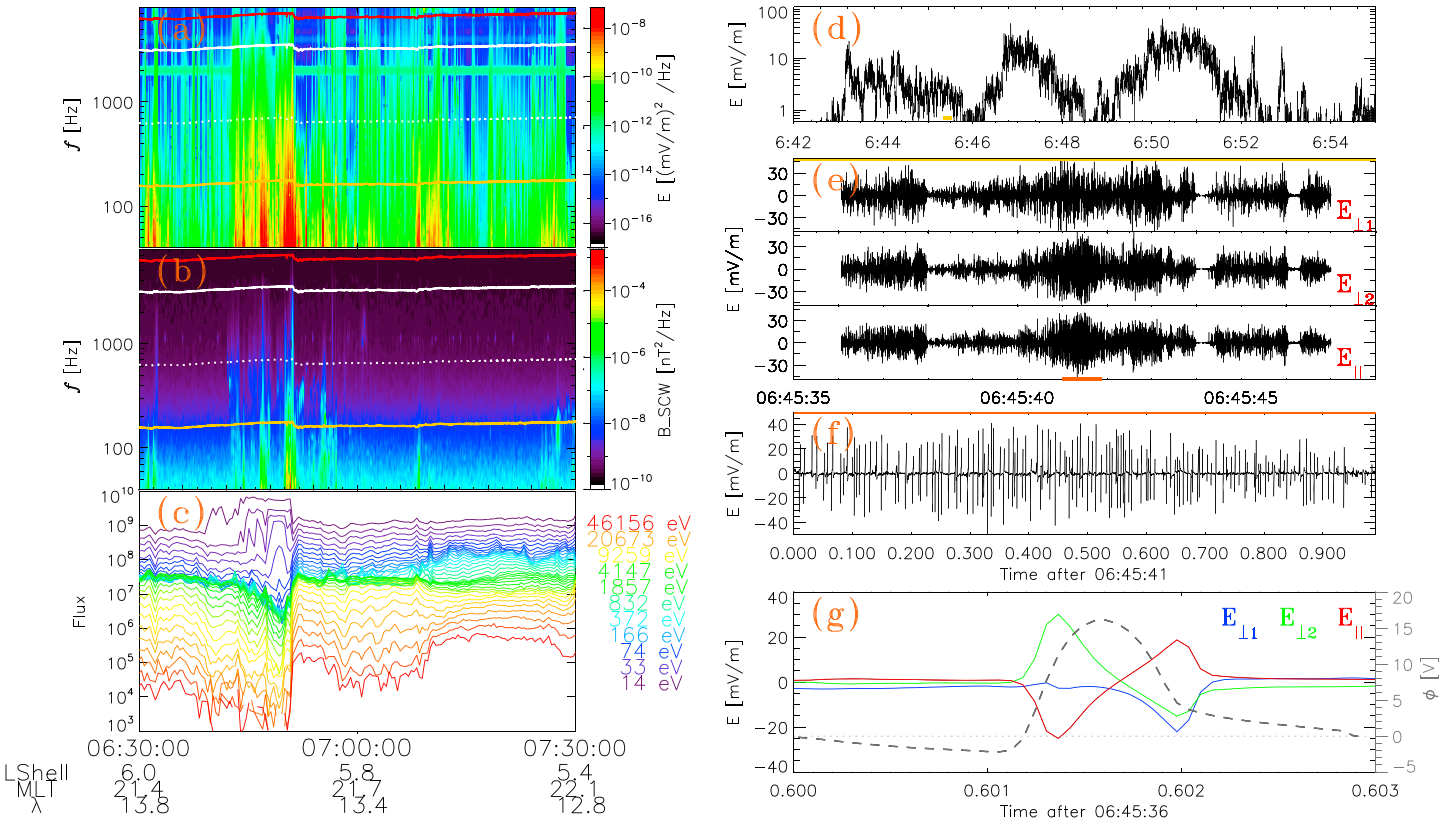


Figure 1. Van Allen Probes observations of one particular injection on 29 June 2013: (a, b) spectrograms of electric and magnetic field fluctuations (red, solid white, and dashed white curves correspond to one, one half, and one tenth of the electron gyrofrequency, while the orange curve corresponds to the low hybrid frequency); (c) electron fluxes; (d) the electric field averaged every 0.125 s over the frequency range [50, 300] Hz; (e) 10 s subinterval (indicated in Figure 1d) of measurements of three electric field components in the burst mode regime (16,384 samples/s); (f) 1 s subinterval (indicated in Figure 1e) of the parallel electric field measurements in the burst mode regime; (g) an expanded view of one of TDS: dashed gray curve shows the electrostatic potential computed as $\int E_{\parallel} V_{\phi} dt$.

We model the EH electrostatic potential Φ with the following three-dimensional Gaussian distribution [*Chen et al.*, 2005; *Vasko et al.*, 2015b]

$$\Phi(z', r) = \Phi_0 \exp\left[-\frac{z'^2}{2d_{\parallel}^2} - \frac{r^2}{2d_{\perp}^2}\right], \quad (1)$$

where Φ_0 and $d_{\parallel,\perp}$ are the EH amplitude and typical parallel and transverse spatial scales, $z' = z - V_{\phi}t$, $r = (x^2 + y^2)^{1/2}$ is the radial distance in the xy plane, $r = 0$ corresponds to the EH symmetry axis, and $z = 0$ corresponds to the spacecraft position. The spacecraft probes an EH at some unknown distance r_* from the EH symmetry axis, and, thus, the potential presented in Figure 1g corresponds to the one-dimensional cut, $\Phi(-V_{\phi}t, r_*)$. We fit this potential to the one-dimensional Gaussian distribution, $\Phi_* \exp(-V_{\phi}^2 t^2/2d_{\parallel}^2)$, and find the best fit parallel scale $d_{\parallel} \sim 0.7$ km. We point out that Φ_* is a lower estimate of the EH amplitude Φ_0, since $\Phi_* = \Phi_0 \exp(-r_*^2/2d_{\perp}^2)$.

Contrary to model (1), Figure 1g demonstrates that peaks of the transverse electric fields are shifted from $E_{\parallel} = 0$. These displacements can be explained by a tilt of the EH symmetry axis with respect to the background magnetic field by a few tens of degrees [*Vasko et al.*, 2015b]. For the sake of simplicity, in our theoretical analysis of the scattering process we assume EHs with the symmetry axis along the background magnetic field.

The transverse scale $d_{\perp}$ of a particular EH cannot be estimated based on single-spacecraft observations because of the unknown parameter r_*. However, the typical scale ratio $d_{\parallel}/d_{\perp}$ can be estimated based on a statistical study of the parallel to transverse electric field ratio [*Ergun et al.*, 1999, 2015]. The transverse scale of EHs in the outer radiation belt is comparable to (or a few times larger than) the parallel scale [*Vasko et al.*, 2017].

Parameters (Φ_0, V_{ϕ}, $d_{\parallel,\perp}$) of EHs observed around the injection front certainly vary in some range. For example, Figure 1d shows that the averaged electric field is larger for the second and third bursts, 6:46–6:48:30 UT

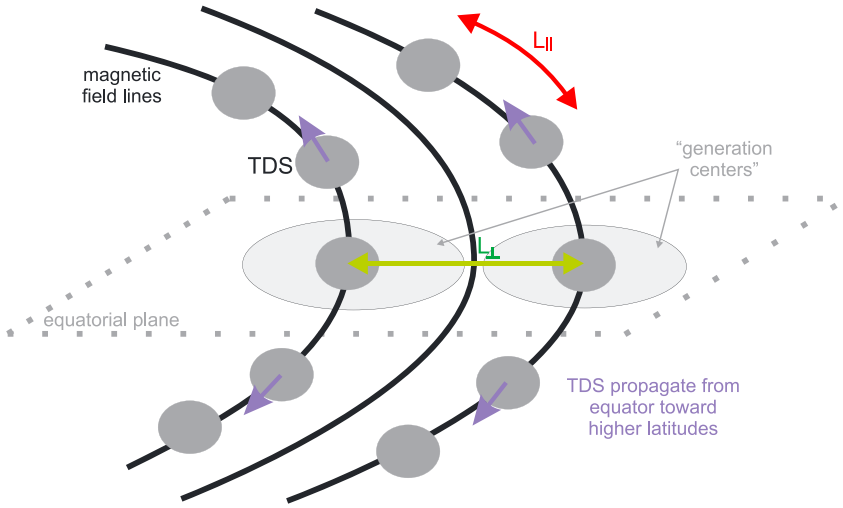


Figure 2. The schematic of the EH spatial distribution: $L_{\parallel}$ is the typical distance between EHs in the direction parallel to the background magnetic field; $L_{\perp}$ is the typical distance between EH generation centers in the direction transverse to the background magnetic field; generation centers are defined as circles in the *xy* plane with the radius of about $2.5d_{\perp}$ (outside a generation center EH electric fields decrease by a factor of more than 20); EHs propagate from the equator toward higher latitudes or in the opposite direction.

and 6:48:30–6:52 UT, than for the first burst, 6:43–6:46 UT. Therefore, EHs should have larger electric fields ($\sim\Phi_0/d_{\parallel}$) and/or are encountered more frequently (larger EH spatial filling factor and/or velocities) for the second and third bursts.

Figure 2 presents the schematics of the EH spatial distribution within an injection. There are indicated average distances $L_{\parallel,\perp}$ between EHs in directions parallel and transverse to the background magnetic field, which determine the EH spatial filling factor $n_{EH} \sim 2/\pi L_{\perp}^2 L_{\parallel}$. The typical time interval between two sequentially observed EHs is less than 10 ms (Figure 1f). During 10 ms the injection front propagates inward by less than about 0.3 km that is smaller than the typical EH transverse scale. Therefore, two sequentially observed EHs are generated in the same "generation center" defined as a circle in the *xy* plane with the radius of about $2.5d_{\perp}$ (outside a generation center the electric field of EHs decreases by more than a factor of 20, $\exp(-2.5^2/2) \sim 1/20$). Therefore, 10 ms time interval corresponds to the magnetic field-aligned spatial separation between EHs. Assuming EH velocities of about 4000 km/s, we find the magnetic field-aligned spatial separation $L_{\parallel} \lesssim 40$ km or $L_{\parallel} \lesssim 50d_{\parallel}$, where we have assumed $d_{\parallel} \sim 0.7$ km.

The 1 s time interval in Figure 1f corresponds to the region with a radial spatial extent of about 25–50 km and may contain at least five generation centers. During the entire 1 s, the typical time interval between EHs is less than 10 ms. Therefore, the distance between generation centers is of about their diameter, $L_{\perp} \sim 5d_{\perp}$ or $L_{\perp} \sim 3.5$ km, if we assume $d_{\perp} \sim 0.7$ km. This is the minimum possible distance between EHs in the transverse direction. Assuming $L_{\parallel} \sim 40$ km, we find the EH spatial filling factor $n_{EH} \sim 2/\pi L_{\perp}^2 L_{\parallel} \sim 10^{-3}$ km^{-3}, so that there is approximately one EH in a cube of 10 km × 10 km × 10 km.

On a time scale of 10 s EHs are observed in groups lasting for a few seconds and separated by a few tenths of seconds (Figure 1e). The time interval of a few tenths of seconds corresponds to a radial spatial extent of about 10 km. Therefore, the distance between generation centers can be sometimes larger than the minimum distance by about 10 km, so that $L_{\perp} \lesssim 15$ km or $L_{\perp} \lesssim 20d_{\perp}$. The corresponding spatial filling factor is $n_{EH} \sim 10^{-4}$ km^{-3}.

3. Electron Interaction With a Single EH

We consider interaction of electrons with a single EH propagating along the background magnetic field. On a time scale of a single interaction the background magnetic field can be assumed to be uniform. The electron dynamics is governed by the following equations

$$\dot{p}_{\parallel} = \partial_z \Phi, \quad \dot{\mathbf{p}}_{\perp} = \nabla_{\perp}\Phi - \omega_c(\mathbf{p}_{\perp} \times \hat{\mathbf{z}}), \tag{2}$$

where $p_\parallel = m_e V_\parallel$ and $\mathbf{p}_\perp = m_e \mathbf{V}_\perp = m_e V_x \hat{\mathbf{x}} + m_e V_y \hat{\mathbf{y}}$ are parallel and transverse momenta (with respect to the background magnetic field $B\hat{\mathbf{z}}$), $\Phi(x, y, z - V_\phi t)$ and V_ϕ are the EH electrostatic potential (in electron volts) and velocity, and ω_c denotes electron gyrofrequency. The evolution of total $W = \mathbf{p}^2/2m_e$ and transverse $W_\perp = \mathbf{p}_\perp^2/2m_e$ kinetic energies is determined by standard equations

$$\frac{dW}{dt} = (\mathbf{V}\cdot\nabla)\Phi = \left(\frac{d\Phi}{dt} - \frac{\partial\Phi}{\partial t}\right)$$
$$\frac{dW_\perp}{dt} = (\mathbf{V}_\perp\cdot\nabla_\perp)\Phi = \left(\frac{d\Phi}{dt} - \frac{\partial\Phi}{\partial t} - V_\parallel\frac{\partial\Phi}{\partial z}\right),$$

where d/dt corresponds to variations along electron trajectory and $\mathbf{V} = V_\parallel\hat{\mathbf{z}} + \mathbf{V}_\perp$. Taking into account that $\partial_t\Phi = -V_\phi\partial_z\Phi$, we find energy variations due to a single interaction

$$\Delta W = V_\phi\int_{-\infty}^{+\infty}\frac{\partial\Phi}{\partial z}dt, \quad \Delta W_\perp = \int_{-\infty}^{+\infty}(V_\phi - V_\parallel)\frac{\partial\Phi}{\partial z}dt\,. \tag{3}$$

We remind the reader that for gyroresonant electrons, $\omega_c d_\parallel(1-\delta_c) \lesssim |V_\parallel - V_\phi| \lesssim \omega_c d_\parallel(1+\delta_c)$, where δ_c determines the resonance width. The first of equation (2) shows that the electron parallel velocity is perturbed as follows, $|V_\parallel - V_\phi| \sim \left(|V_\parallel - V_\phi|_\infty^2 + 2\Phi/m_e\right)^{1/2}$, where $|V_\parallel - V_\phi|_\infty$ corresponds to the parallel electron velocity at large distances from EH. In the case of isolated resonances, $\Delta_{LC} = \omega_c d_\parallel/\Delta V_L \gg 1$, the parallel velocity variation of gyroresonant electrons can be neglected, $|V_\parallel - V_\phi| \approx$ const. Neglecting $V_\parallel$ variation in the second of equations (3), we find

$$\Delta W = \frac{V_\phi}{V_\phi - V_\parallel}\Delta W_\perp, \quad \Delta W_\perp = (V_\phi - V_\parallel)\int_{-\infty}^{+\infty}\frac{\partial\Phi}{\partial z}dt\,. \tag{4}$$

The ratio of $\nabla_\perp\Phi$ to the Lorentz force in equation (2) is of the order of $V_E/V_\perp$, where V_E is the typical cross-field drift velocity. We note that $V_E/V_\perp \sim \Delta V_L/\Delta_{LC}V_\perp \ll 1$ for electrons with energies $W \gg \Phi_0/\Delta_{LC}^2$. The typical background magnetic field $B \sim 140$ nT, EH amplitude $\Phi_0 \sim 30$ eV, and parallel scale $d_\parallel \sim 0.7$ km result in $\Delta_{LC} \sim 5$. Thus, the transverse dynamics of electrons with energies $W \gg \Phi_0/\Delta_{LC}^2 \sim 1$ eV is only slightly perturbed and the integral in equation (4) can be evaluated along unperturbed electron trajectories (analog of the quasi-linear approximation). The detailed calculation of $\Delta W_\perp$ for EHs with the Gaussian electrostatic potential (1) is given in Appendix A.

Taking into account that $W_\perp = W\sin^2\alpha$, where α is a local pitch angle, we find the local pitch angle variation due to a single interaction

$$\Delta\alpha = \frac{V_\phi\cos^2\alpha - V_\parallel}{V_\phi - V_\parallel}\frac{\Delta W_\perp}{W\sin(2\alpha)}, \tag{5}$$

while the momentum variation is unambiguously related to the pitch angle variation [*Lyons*, 1974]

$$\frac{\Delta p}{p} = \frac{V_\phi\sin\alpha\cos\alpha}{V_\phi\cos^2\alpha - V_\parallel}\Delta\alpha\,. \tag{6}$$

The pitch angle variation $\Delta\alpha$ depends on the electron energy W, local pitch angle α, and parameters illustrated in Figure 3: distance ρ between the EH symmetry axis and electron guiding center; angle ψ setting electron guiding center position in the xy plane; angle φ setting electron initial gyrophase. Let us consider an ensemble of electrons with uniformly distributed initial gyrophases. Averaging over the ensemble, we find $\langle\Delta\alpha\rangle_\varphi = 0$, while $\langle\Delta\alpha^2\rangle_\varphi \neq 0$ and depends on W, α, and ρ as follows (see Appendix A for $\langle\Delta W_\perp\rangle_\varphi$ expression)

$$\langle\Delta\alpha^2\rangle_\varphi = \frac{4\pi\Phi_0^2}{W^2\sin^2(2\alpha)}\left(\frac{V_\parallel - V_\phi\cos^2\alpha}{V_\parallel - V_\phi}\right)^2\left(\frac{\omega_c d_\parallel}{V_\parallel - V_\phi}\right)^2$$
$$\cdot\exp\left[-\frac{\rho^2+\rho_L^2}{d_\perp^2}\right]\sum_{n=1}^{\infty}n^2 I_n^2\left(\frac{\rho\rho_L}{d_\perp^2}\right)\exp\left[-\frac{n^2\omega_c^2 d_\parallel^2}{(V_\parallel - V_\phi)^2}\right], \tag{7}$$

where $\rho_L = V_\perp/\omega_c$ is electron gyroradius, $V_\parallel = (2W/m_e)^{1/2}\cos\alpha$, $V_\perp = (2W/m_e)^{1/2}\sin\alpha$, and I_n is the nth order modified Bessel function. EH can be thought of as a packet of planar electrostatic waves with different wavenumbers ($d_\parallel^{-1}$ is the typical parallel wavenumber) propagating with the same velocity V_ϕ at different wave-normal angles. As shown in Appendix A, each term of the series (7) corresponds to scattering by electrostatic waves in the nth order cyclotron resonance with a given electron. Making use of equation (6),

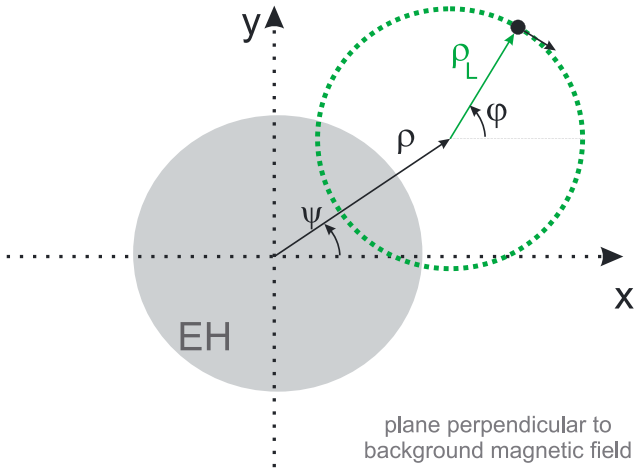


Figure 3. The schematic of interaction process between electron and EH presented in the plane perpendicular to the background magnetic field. The interaction process depends on indicated parameters: distance ρ between EH and electron guiding center, angle ψ setting electron guiding center position in the xy plane, and angle φ corresponding to electron initial gyrophase. The parameter ρ_L denotes electron gyroradius.

we find zero ensemble-averaged momentum variation, $\langle \Delta p \rangle_\varphi = 0$. Once $\langle \Delta\alpha^2 \rangle_\varphi$ is calculated, the corresponding momentum and mixed variations are determined straightforwardly [*Lyons*, 1974]

$$\frac{\langle \Delta p^2 \rangle_\varphi}{p^2} = \left(\frac{V_\phi \sin\alpha \cos\alpha}{V_\phi \cos^2\alpha - V_\parallel} \right)^2 \langle \Delta\alpha^2 \rangle_\varphi$$
$$\frac{\langle \Delta p \Delta\alpha \rangle_\varphi}{p} = \frac{V_\phi \sin\alpha \cos\alpha}{V_\phi \cos^2\alpha - V_\parallel} \langle \Delta\alpha^2 \rangle_\varphi . \tag{8}$$

The pitch angle variation (7) depends on the distance ρ between EH and electron guiding center. Let us consider an ensemble of electrons with guiding centers uniformly distributed within a circle of radius R_0. We average equation (7) over guiding center positions and find that $\langle \Delta\alpha^2 \rangle_{\varphi,\rho} \equiv \langle \Delta\alpha^2 \rangle$ depends on the energy and pitch angle as follows

$$\langle \Delta\alpha^2 \rangle = \frac{4\pi\Phi_0^2}{W^2 \sin^2(2\alpha)} \left(\frac{V_\parallel - V_\phi \cos^2\alpha}{V_\parallel - V_\phi} \right)^2 \left(\frac{d_\perp}{R_0} \right)^2 \cdot \left(\frac{\omega_c d_\parallel}{V_\parallel - V_\phi} \right)^2 \cdot \sum_{n=1}^{\infty} n^2 \Lambda_n^s(\kappa) \exp\left[-\frac{n^2 \omega_c^2 d_\parallel^2}{(V_\parallel - V_\phi)^2} \right] , \tag{9}$$

where $s = R_0^2/d_\perp^2$, $\kappa = \rho_L/d_\perp = V_\perp/\omega_c d_\perp$ and

$$\Lambda_n^s(\kappa) = e^{-\kappa^2} \int_0^s e^{-x} I_n^2(\kappa\sqrt{x}) \mathrm{d}x . \tag{10}$$

The corresponding momentum and mixed variations, $\langle \Delta p^2 \rangle$ and $\langle \Delta p \Delta\alpha \rangle$, are determined straightforwardly from equation (8). We introduce normalized units $w = W/W_c$ and $v_\phi = V_\phi/\omega_c d_\parallel$, where $W_c = m_e \omega_c^2 d_\parallel^2/2$ is the typical energy of gyroresonant electrons. The normalized velocity v_ϕ can be considered as a ratio of the effective EH frequency $V_\phi/d_\parallel$ to the electron gyrofrequency. In normalized units we have

$$\langle \Delta\alpha^2 \rangle = \frac{\pi\Phi_0^2}{W_c^2} \frac{\left(\sqrt{w} - v_\phi \cos\alpha \right)^2}{w^2 \sin^2\alpha \left(\sqrt{w}\cos\alpha - v_\phi \right)^4} \left(\frac{d_\perp}{R_0} \right)^2 \cdot \sum_{n=1}^{\infty} n^2 \Lambda_n^s(\kappa) \exp\left[-\frac{n^2}{\left(\sqrt{w}\cos\alpha - v_\phi \right)^2} \right] , \tag{11}$$

where $\kappa = \rho_L/d_\perp = \sin\alpha \sqrt{w} d_\parallel/d_\perp$. The specific functional form of $\langle \Delta\alpha^2 \rangle$ given by equation (11) is certainly due to the Gaussian model (1). Other models could be used to obtain quantitatively similar results.

Figure 4 presents $\langle \Delta\alpha^2 \rangle$ and $\langle \Delta p^2 \rangle/p^2$ obtained via equations (8) and (11) for electrons in the energy range $W \sim (0.1\text{–}100)\ W_c$ and guiding centers uniformly distributed within a circle of radius $R_0 = 5d_\perp$. We have assumed a spherical EH, $d_\parallel = d_\perp$, with $\Phi_0 = 0.03\ W_c$ and $v_\phi \sim 0.2$. These normalized parameters correspond, for example, to rather typical EHs with amplitude $\Phi_0 \sim 30$ eV, spatial scale $d_\parallel \sim 0.75$ km

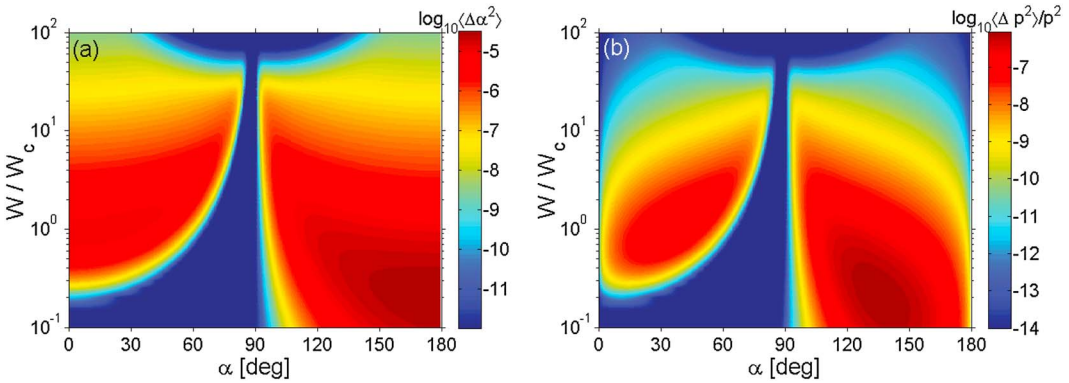


Figure 4. The ensemble-averaged local pitch angle and momentum variations due to a single interaction with EH as calculated via analytical formulas (8) and (11) (see for details section 3). W_c is the typical energy of gyroresonant electrons.

(electric field amplitude is about 30 mV/m), and velocity $V_\phi \sim 4000$ km/s in the background magnetic field $B \sim 140$ nT.

In this case $W_c \sim 1$ keV, so that electrons under consideration are in the energy range $W \sim 0.1-100$ keV. The overlapping parameter is $\Delta_{LC} \sim 5$, so that resonances can be assumed isolated. We have determined the pitch angle and momentum variations by summing 15 terms of series (11).

The pitch angle and momentum scattering are most efficient for electrons with energy $W \sim W_c$ at $\alpha < 90°$ and for lower energy electrons at $\alpha > 90°$. The reason for this asymmetry is that at $\alpha > 90°$ the gyroresonance condition, $V_\parallel - V_\phi \sim \pm\omega_c d_\parallel$, is met for lower energy electrons. The maximum pitch angle variation is $\langle\Delta\alpha^2\rangle \sim 2.5 \cdot 10^{-5}$ or, equivalently, $\langle\Delta\alpha^2\rangle^{1/2} \sim 0.3°$. The momentum variation is about 2 orders of magnitude smaller with the maximum $\langle\Delta p^2\rangle/p^2 \sim 2 \cdot 10^{-7}$. This is, as shown previously for linear plasma modes [*Kennel and Engelmann*, 1966; *Lyons*, 1974], due to the effective EH frequency $V_\phi/d_\parallel$ much smaller than the electron gyrofrequency ($v_\phi = V_\phi/\omega_c d_\parallel = 0.2$). Note that nonpropagating EHs, $v_\phi = 0$, could drive only pitch angle scattering.

Figure 5 presents analytical curves corresponding to the sums of one, five, and ten terms of series (11) for several different electron energies. The sum of series (11) is well reproduced by the first term for electrons with energies $W \lesssim W_c$. The larger number of terms, $n \sim (W/W_c)^{1/2}$, should be taken into account for higher-energy electrons capable to meet higher-order cyclotron resonances with planar electrostatic waves contributing to the Fourier expansion of the EH electrostatic field (see Appendix A).

We verify theoretical equation (11) by making use of the test particle simulation. We solve equation (2) numerically for an ensemble of 10^5 electrons with some fixed initial energy. Electron guiding centers are distributed uniformly within a circle with radius $R_0 = 5d_\perp$ in the xy plane, while the EH center is placed at the origin of the coordinate system. Electrons with $V_\parallel < V_\phi$and $V_\parallel > V_\phi$ are initially placed at large distance from EH, $z = 10d_\parallel$ and $z = -10d_\parallel$, respectively, so that interaction could take place. Figure 6 presents results of the test particle simulation for electrons with energy $W = W_c$ and EH parameters assumed above ($\Phi_0 = 0.03W_c$, $d_\parallel = d_\perp$, and $v_\phi = 0.2$). Figure 6a presents the distribution of electrons in the xy plane at the initial moment. Figure 6b presents a scatterplot of pitch angle variations in dependence on the distance between EH center and electron guiding center. The most efficient pitch angle scattering occurs at some distance from the EH, where the transverse electric field is maximum. Figure 6c presents a scatterplot of pitch angle variations as well as the ensemble-averaged $\langle\Delta\alpha^2\rangle^{1/2}$ in dependence on α.

In Figure 5 we compare $\langle\Delta\alpha^2\rangle$ calculated via the test particle simulation and analytically via equation (11). There is a good agreement between test particle and analytical curves at energies $W \gtrsim 0.1W_c$. The slightly worse agreement at $W = 0.05W_c$ is due to a partial overlapping of the gyroresonance with the Landau resonance and, hence, worse applicability of the assumption $|V_\parallel - V_\phi| \approx$ const. In the case of a partial overlapping, the assumption $|V_\parallel - V_\phi| \approx$ const underestimates the time scale of the EH crossing, since $|V_\parallel - V_\phi| \sim \left(|V_\parallel - V_\phi|_\infty^2 + 2\Phi/m_e\right)^{1/2} > |V_\parallel - V_\phi|_\infty$ due to positive EH potential. Therefore, the number of cyclotron rotations performed by electrons during the EH crossing is overestimated resulting in underestimation of the electron pitch angle variation. We conclude that theoretical equations (9) and (11) can be used to

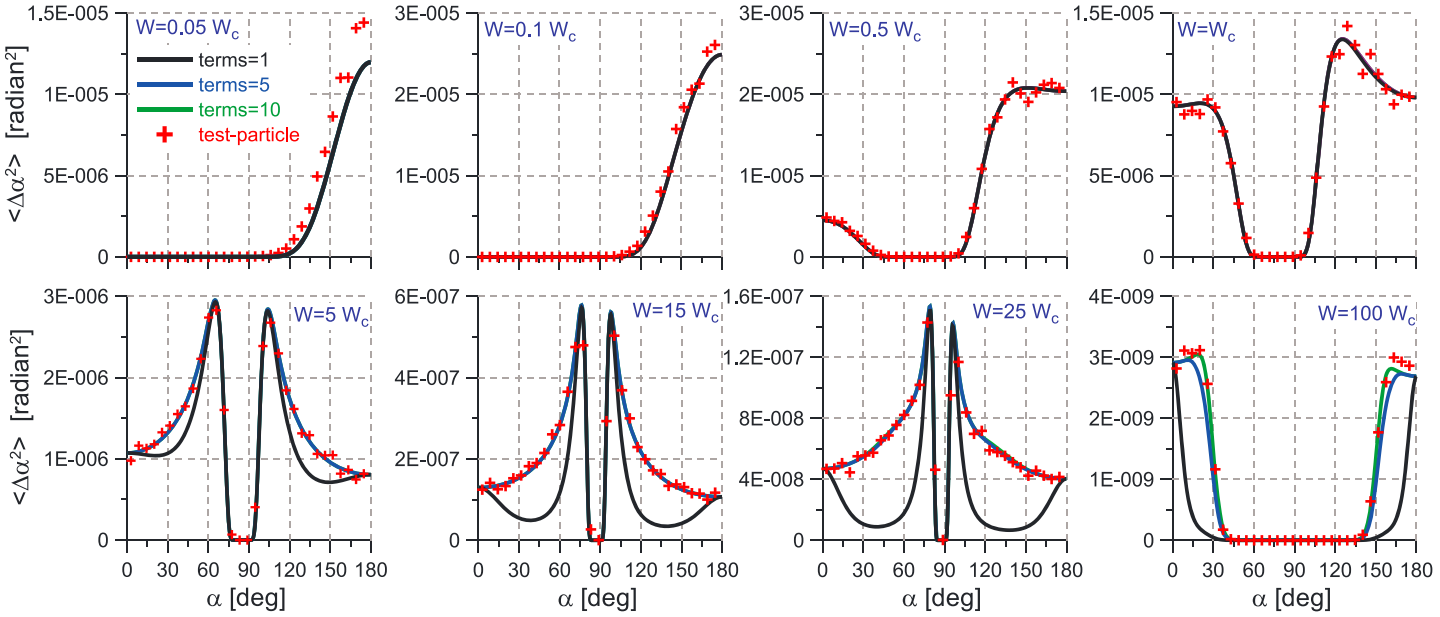


Figure 5. Different curves correspond to sum of one, five, and ten terms in series (11) providing the ensemble-averaged pitch angle variation due to a single interaction with EH. The pitch angle variations calculated via the test particle simulation are presented by red crosses. W_c is the typical energy of gyroresonant electrons (see for details section 3).

describe the local pitch angle scattering by a single EH for electrons with not too low energies (in comparison with W_c), while for low-energy electrons these formulas provide lower estimates. The same conclusions are true with respect to theoretical estimates for $\langle \Delta p^2 \rangle$ and $\langle \Delta p \Delta \alpha \rangle$.

The formulas derived above can be applied to analyze the role of EHs in quite different space plasma systems (auroral region, reconnecting current sheets, shock waves, etc.) characterized by some specific distribution of the background magnetic field and EH parameters. In the next section we apply these formulas to quantify the role of EHs observed around injection fronts in the outer radiation belt.

4. Interaction With Many EHs and Bounce-Averaged Diffusion Coefficients

In the course of the cyclotron rotation at some latitude, an electron interacts with many EHs distributed in the plane perpendicular to the background magnetic field. The average number of EHs per square dS in this plane is $dS/\pi L_\perp^2$, where $L_\perp$ is the average distance between EH generation centers. The number of EHs at distance $(\rho,\ \rho + d\rho)$ from electron guiding center is $2\pi\rho d\rho/\pi L_\perp^2$. The pitch angle variation due to interaction with each

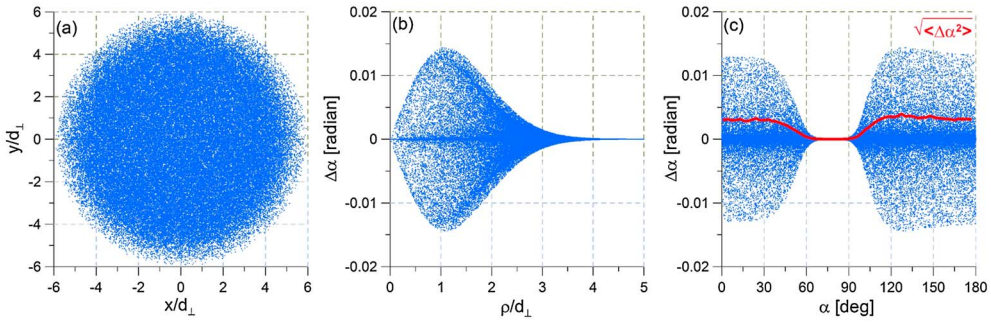


Figure 6. The illustration of the test particle simulation for electrons with initial energy $W = W_c$. The numerical integration of equation (2) is performed for 10^5 electrons interacting with a spherical EH with amplitude $\Phi_0 = 0.03 W_c$ and normalized velocity $v_\phi = V_\phi/\omega_c d_\parallel = 0.2$: (a) distribution of electrons at the initial moment in the xy plane; (b) the pitch angle variation (due to a single interaction) in dependence on the initial distance ρ between electron guiding center and EH; (c) the pitch angle variation in dependence on the initial pitch angle. Red curve represents root mean square pitch angle variation in dependence on the initial pitch angle.

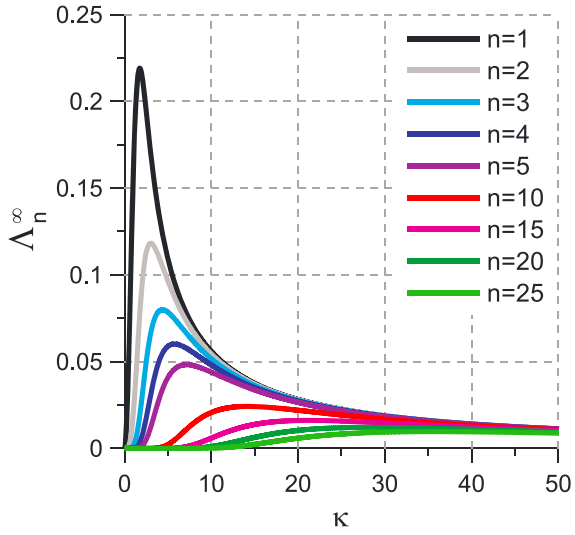


Figure 7. Functions $\Lambda_n^\infty(\kappa)$ calculated numerically (see equation (10)) and used to calculate the diffusion coefficients (see equation (13)).

of these EHs (averaged over gyrophases) is given by equation (7) and depends on the distance ρ between EH and electron guiding center. The pitch angle variation due to interaction with many EHs at some fixed latitude is $\langle\Delta\alpha^2\rangle = L_\perp^{-2}\int_0^{+\infty}\langle\Delta\alpha^2\rangle_\varphi\, d\rho^2$ and can be written in the following form

$$\langle\Delta\alpha^2\rangle = \frac{4\pi\Phi_0^2}{W^2\sin^2(2\alpha)}\left(\frac{V_\parallel - V_\phi\cos^2\alpha}{V_\parallel - V_\phi}\right)^2\left(\frac{d_\perp}{L_\perp}\right)^2\cdot\left(\frac{\omega_c d_\parallel}{V_\parallel - V_\phi}\right)^2\cdot\sum_{n=1}^{\infty} n^2\Lambda_n^\infty(\kappa)\exp\left[-\frac{n^2\omega_c^2 d_\parallel^2}{(V_\parallel - V_\phi)^2}\right]. \quad (12)$$

It can be shown that $\Lambda_n^\infty(\kappa)$ determined by equation (10) satisfy the recurrence relation $\kappa^2\left(\Lambda_{n+1}^\infty - \Lambda_{n-1}^\infty\right) = -4n\Lambda_n^\infty$, simplifying calculation of these coefficients presented in Figure 7 for several values of n.

In the course of the bounce motion between magnetic mirror points, electrons interact with EHs at different latitudes. The distribution of EHs along the magnetic field lines is characterized by the average distance $L_\parallel$ between them. The time interval between two sequential interactions is $\Delta t = L_\parallel/|V_\parallel - V_\phi|$. Taking into account equation (12), the local pitch angle diffusion coefficient $D_{\alpha\alpha} = \langle\Delta\alpha^2\rangle/2\Delta t$ can be written in the form

$$D_{\alpha\alpha} = 2\pi\omega_c\frac{d_\parallel d_\perp^2}{L_\parallel L_\perp^2}\frac{\Phi_0^2}{W^2\sin^2(2\alpha)}\left(\frac{V_\parallel - V_\phi\cos^2\alpha}{V_\parallel - V_\phi}\right)^2\frac{\omega_c d_\parallel}{|V_\parallel - V_\phi|}\sum_{n=1}^{\infty} n^2\Lambda_n^\infty(\kappa)\exp\left[-\frac{n^2\omega_c^2 d_\parallel^2}{(V_\parallel - V_\phi)^2}\right].$$

As expected the diffusion coefficient is proportional to the EH spatial filling factor $n_{EH} \sim 2/\pi L_\perp^2 L_\parallel$ and to the square of EH amplitude Φ_0.

In this paper we analyze electron scattering assuming identical (independent of latitude) parameters for all EHs. We introduce the typical energy of gyroresonant electrons $W_0 = m_e\omega_0^2 d_\parallel^2/2$ and use the normalized energy $w = W/W_0$, where ω_0 is electron gyrofrequency at the equator, $\omega_c = \omega_0 b(\lambda)$ is electron gyrofrequency at latitude λ, and $b(\lambda)$ determines the magnetic field variation with latitude. We introduce the normalized EH velocity $v_0 = V_\phi/\omega_0 d_\parallel$ that is also a ratio of the effective EH frequency $V_\phi/d_\parallel$ and electron gyrofrequency at the equator. In normalized units the local pitch angle diffusion coefficient can be written in the following form

$$D_{\alpha\alpha} = D_0\frac{\left(\sqrt{w} - v_0\cos\alpha\right)^2 b^2(\lambda)}{w^2\sin^2\alpha\,|\sqrt{w}\cos\alpha - v_0|^3}\sum_{n=1}^{\infty} n^2\Lambda_n^\infty(\kappa)\exp\left[-\frac{n^2 b^2(\lambda)}{\left(\sqrt{w}\cos\alpha - v_0\right)^2}\right], \quad (13)$$

where

$$D_0 = \frac{\pi\omega_0}{2}\frac{d_\parallel d_\perp^2}{L_\parallel L_\perp^2}\frac{\Phi_0^2}{W_0^2}, \quad \kappa = \frac{\rho_L}{d_\perp} = \frac{\sqrt{w}\sin\alpha}{b(\lambda)}\frac{d_\parallel}{d_\perp}. \quad (14)$$

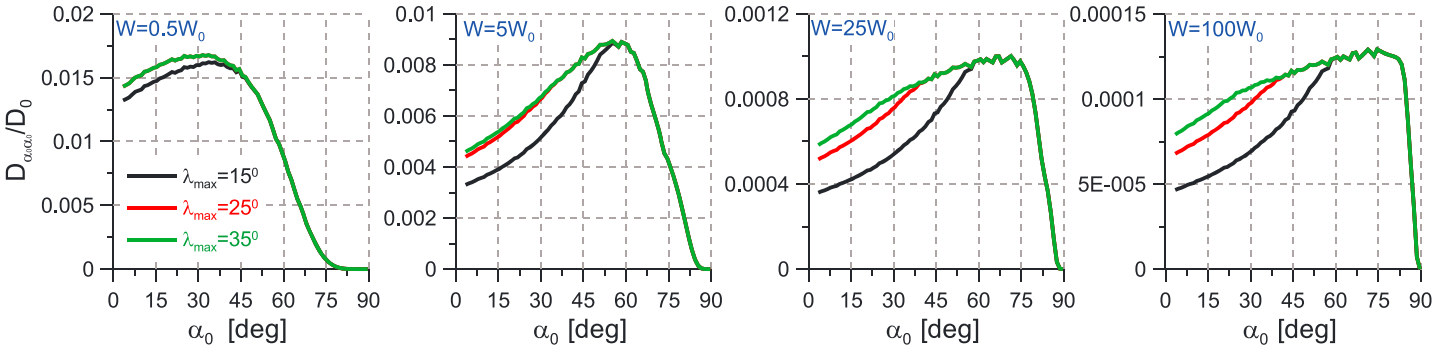


Figure 8. The normalized bounce-averaged pitch angle diffusion coefficients at several energies in dependence on the maximum latitude λ_{max} below which EHs are concentrated. EHs are assumed to be spherical with the normalized velocity $v_0 = 0.2$. W_0 is the typical energy of electrons gyroresonant with EHs at the equator.

The local momentum and mixed diffusion coefficients, D_{pp} and $D_{p\alpha}$, are determined as [*Lyons*, 1974]

$$p^{-1}D_{p\alpha} = -\frac{v_0 \sin\alpha}{\sqrt{w} - v_0 \cos\alpha} D_{\alpha\alpha}, \quad p^{-2}D_{pp} = \left(\frac{v_0 \sin\alpha}{\sqrt{w} - v_0 \cos\alpha}\right)^2 D_{\alpha\alpha}\,.$$

The bounce-averaged diffusion coefficients dependent on the equatorial pitch angle α_0 and energy W are calculated via the standard averaging procedure [*Lyons et al.*, 1972; *Glauert and Horne*, 2005]:

$$D_{\alpha_0\alpha_0} = \frac{1}{T_b}\oint D_{\alpha\alpha}\left(\frac{\partial\alpha_0}{\partial\alpha}\right)^2 \mathrm{d}t, \quad D_{p\alpha_0} = \frac{1}{T_b}\oint D_{p\alpha}\left(\frac{\partial\alpha_0}{\partial\alpha}\right)\mathrm{d}t, \quad D_{pp} = \frac{1}{T_b}\oint D_{pp}\mathrm{d}t\,, \tag{15}$$

where $T_b(W, \alpha_0)$ is the bounce period. The local and equatorial pitch angles are related via

$$b(\lambda)\sin^2\alpha_0 = \sin^2\alpha, \quad \partial\alpha_0/\partial\alpha = \tan\alpha_0/\tan\alpha\,.$$

We assume the dipole background magnetic field, $b(\lambda) = \sqrt{1+3\sin^2\lambda}/\cos^6\lambda$. The nondipole magnetic field may influence the bounce-averaged diffusion coefficients [*Orlova and Shprits*, 2010; *Ni et al.*, 2011c], but we leave this question for future studies. The integration in equation (15) is transformed into integration with respect to the magnetic latitude by taking into account that $\mathrm{d}t = LR_E\cos\lambda\sqrt{1+3\sin^2\lambda}\,\mathrm{d}\lambda/V\cos\alpha$, where R_E denotes the Earth radius [*Lyons et al.*, 1972]. EHs are assumed to be concentrated below some latitude, $|\lambda| \le \lambda_{max}$, so that in equation (15) we assume $D_{\alpha\alpha} = 0$ at $|\lambda| > \lambda_{max}$.

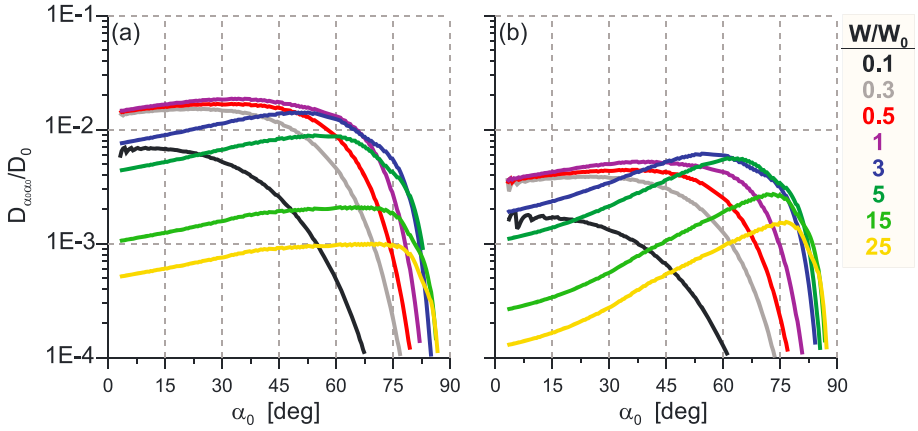


Figure 9. The normalized bounce-averaged pitch angle diffusion coefficients computed for EHs with normalized velocity $v_0 = 0.2$ and different parallel to transverse scale ratios: (a) $d_\perp = d_\parallel$ and (b) $d_\perp = 2d_\parallel$. W_0 is the typical energy of electrons gyroresonant with EHs at the equator.

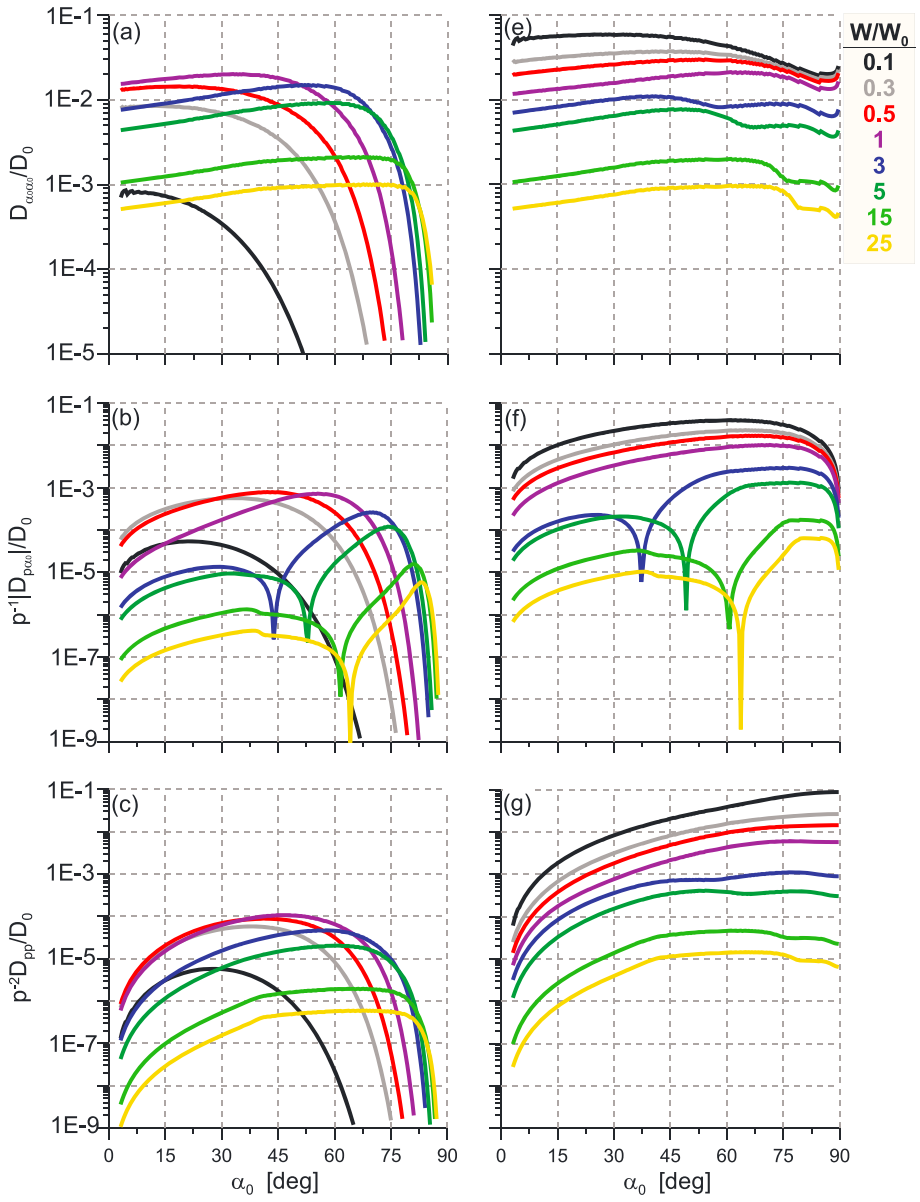


Figure 10. The normalized bounce-averaged diffusion coefficients computed for EHs with normalized velocities (a–c) $v_0 = 0.1$ and (e–f) $v_0 = 0.5$. W_0 is the typical energy of electrons gyroresonant with EHs at the equator.

The bounce-averaged diffusion coefficients depend on the EH amplitude Φ_0 and EH spatial filling factor via the multiplicative factor D_0. The normalized diffusion coefficients, $D_{\alpha_0\alpha_0}/D_0$, etc., depend on the equatorial pitch angle α_0, normalized energy $w = W/W_0$, maximum latitude λ_{max}, normalized EH velocity v_0, and parallel to transverse scale ratio $d_\parallel/d_\perp$.

Figure 8 demonstrates normalized pitch angle diffusion coefficients computed for EHs concentrated below 15°, 25°, and 35°. We have assumed that EHs are spherical ($d_\parallel/d_\perp = 1$) with the normalized velocity $v_0 = 0.2$. As expected the latitudinal extent of EHs largely influences electrons with small pitch angles, $\alpha_0 < 60°$, and higher-energy electrons capable to meet the gyroresonance condition at higher latitudes. Overall, variation of the latitudinal extent of EHs from $|\lambda| < 15°$ to $|\lambda| < 35°$ changes the diffusion coefficients near the loss cone by a factor of less than 2. Since EHs are observed at all latitudes covered by Van Allen Probes, $|\lambda| \lesssim 18°$, in what follows, we compute diffusion coefficients assuming $\lambda_{max} = 25°$.

Figure 9 demonstrates normalized pitch angle diffusion coefficients computed for spherical and nonspherical ($d_\perp/d_\parallel = 2$) EHs for several energies W/W_0. EH velocities are the same as above, $v_0 = 0.2$. The scattering

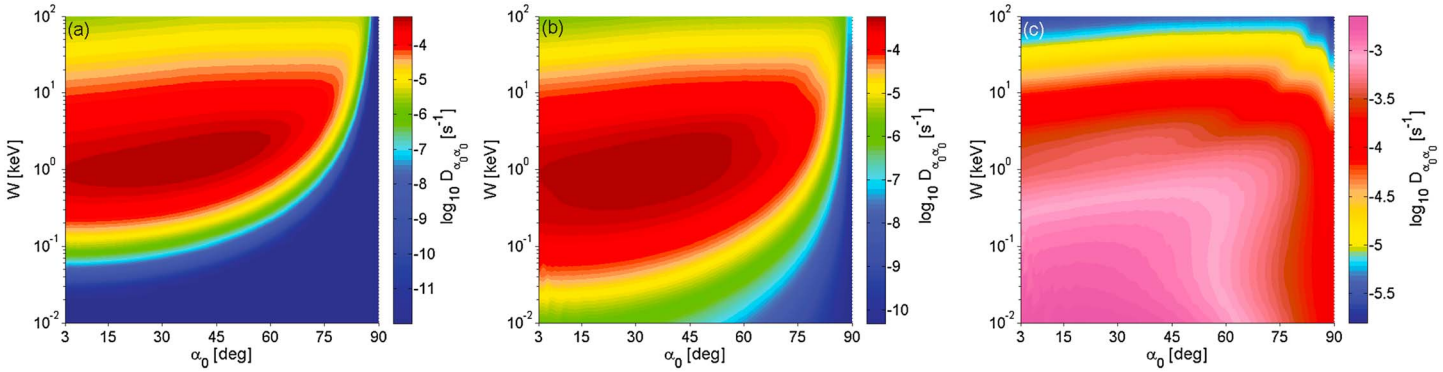


Figure 11. The bounce-averaged pitch angle diffusion coefficients computed for EHs with the parallel scale $d_{||} = 0.75$ km and different velocities: (a) $V_\phi = 1000$ km/s, (b) $V_\phi = 4000$ km/s, and (c) $V_\phi = 8000$ km/s.

should obviously disappear for one-dimensional EHs, $d_\perp = \infty$. In accordance with this, the pitch angle scattering driven by nonspherical EHs with $d_\perp/d_{||} > 1$ is less efficient than the scattering driven by spherical EHs. The comparison of Figures 9a and 9b shows that the increase of $d_\perp/d_{||}$ by a factor of 2 results in decrease of the scattering rates near the loss cone by a factor of about 4. In what follows, we present diffusion coefficients computed for spherical EHs.

Figure 10 demonstrates normalized pitch angle, momentum, and mixed diffusion coefficients computed for EHs with velocities $v_0 = 0.1$ and $v_0 = 0.5$. The pitch angle scattering by slow EHs is most efficient for electrons with energies $W \sim W_0$ and at pitch angles $\alpha_0 \lesssim 60°$. The pitch angle scattering rate significantly decreases toward $\alpha_0 \sim 90°$. The effective frequency of slow EHs is much smaller than the electron gyrofrequency resulting in momentum (mixed) scattering 2 (1) orders of magnitude less efficient than the pitch angle scattering (in accordance with *Lyons* [1974]). The scattering driven by faster EHs exhibits quite different properties. First, there is 2 orders of magnitude more efficient pitch angle scattering for electrons with energies of a few tenths of W_0. This substantial increase of the scattering rates occurs, because lower energy electrons can meet the gyroresonance condition with faster EHs. Second, the pitch angle scattering of equatorial electrons, $\alpha_0 \sim 90°$, becomes quite efficient. Third, the effective frequency of faster EHs is comparable to the electron gyrofrequency resulting in comparable momentum, mixed, and pitch angle scattering rates. The most efficient momentum scattering occurs for equatorial electrons, $\alpha_0 \sim 90°$. Overall, faster EHs are more efficient for energization and loss of electrons at lower energies. Figures 8–10 demonstrate that the latitudinal extent of EHs influences the normalized diffusion coefficients much less than the EH parameters.

5. Realistic Bounce-Averaged Diffusion Coefficients

In this section we demonstrate the pitch angle diffusion coefficients computed for EHs with amplitudes $\Phi_0 = 30$ eV; the magnetic field-aligned separation between EHs, $L_{||} = 50 d_{||}$; and the minimum possible separation in the transverse direction, $L_\perp = 5 d_\perp$. We demonstrate variations of the diffusion coefficients with the EH parallel scale and velocity as well as L shell. We remind the reader that in this paper we assume the dipole background magnetic field.

Figure 11 demonstrates pitch angle diffusion coefficients computed for EHs with the parallel scale $d_{||} = 0.75$ km and different velocities $V_\phi = 1000$, 4000, and 8000 km/s at L shell $L = 6$. Slow EHs efficiently scatter 0.5–2 keV electrons at the maximum scattering rate $D_{\alpha_0\alpha_0} \sim 3 \cdot 10^{-4}$ s^{-1}. EHs with moderate velocities, $V_\phi = 4000$ km/s, efficiently scatter 0.2–2 keV electrons at similar maximum scattering rate. Fast EHs efficiently scatter $\lesssim$1 keV electrons at rates $D_{\alpha_0\alpha_0} \sim 10^{-3}$ to $3 \cdot 10^{-2}$ s^{-1}, while the scattering of 1–3 keV electrons occurs at rates $D_{\alpha_0\alpha_0} \sim 3 \cdot 10^{-4}$–$10^{-3}$ s^{-1}. The higher velocities result in higher normalized velocities v_0. Therefore, Figure 11 demonstrates the same effect as Figures 10a and 10e but in the form of two-dimensional maps.

Figure 12 demonstrates pitch angle diffusion coefficients computed for EHs with moderate velocities $V_\phi = 4000$ km/s and different parallel scales $d_{||} = 0.3$, 0.75 and 1.3 km (transverse scale varies coherently due to our assumption of spherical EHs) at L shell $L = 6$. EHs with smaller parallel scales efficiently scatter $\lesssim$ 1 keV as well as about 1–8 keV electrons at rates $D_{\alpha_0\alpha_0} \sim 3 \cdot 10^{-3}$ to $2 \cdot 10^{-2}$ s^{-1} and $D_{\alpha_0\alpha_0} \sim 3 \cdot 10^{-4}$ to $3 \cdot 10^{-3}$ s^{-1}, respectively. EHs with moderate parallel scales efficiently scatter 0.2–2 keV electrons at rate $D_{\alpha_0\alpha_0} \sim 3 \cdot 10^{-4}$ s^{-1}. EHs with

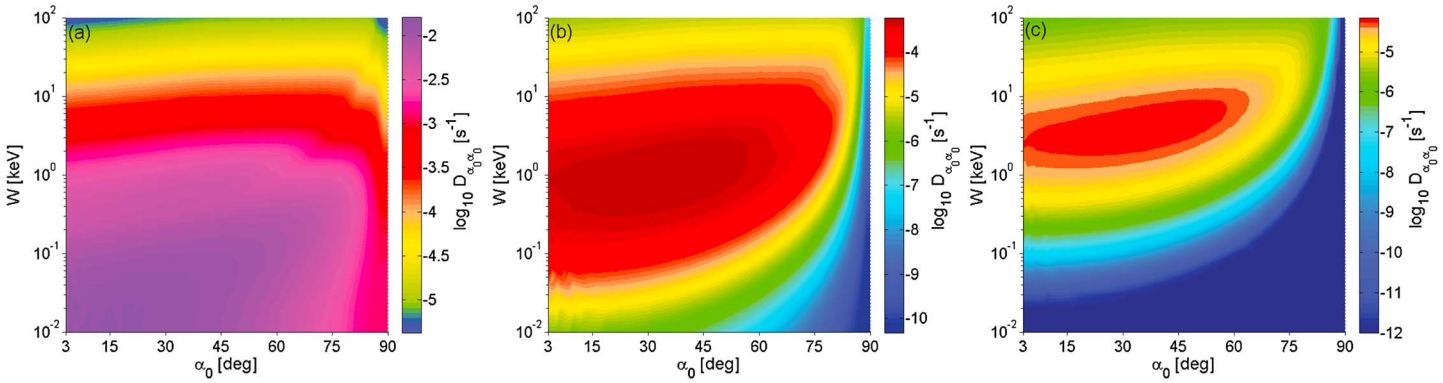


Figure 12. The bounce-averaged pitch angle diffusion coefficients computed for spherical EHs with the velocity $V_\phi = 4000$ km/s and different parallel scales: (a) $d_\parallel = 0.3$, (b) $d_\parallel = 0.75$ km, and (c) $d_\parallel = 1.3$ km.

larger parallel scales provide efficient scattering of about 2–5 keV electrons at rate $D_{\alpha_0\alpha_0} \sim 3 \cdot 10^{-5}\,s^{-1}$. The increase of EH parallel scales increases the energy of most efficiently scattered electrons, since the typical energy of gyroresonant electrons $W_0 \propto d_\parallel^2$. The variation of EH parallel scales also results in variation of the normalized velocity $v_0 \propto d_\parallel^{-1}$ and of the multiplicative factor $D_0 \propto (\Phi_0/W_0)^2 \propto d_\parallel^{-4}$ (note that $L_\parallel$ and $L_\perp$ are varied coherently with $d_\parallel$, so that $d_\parallel d_\perp^2/L_\parallel L_\perp^2 = \text{const}$). The decrease of EH parallel scales by a factor of 2 results in increase of both v_0 and D_0 by factors of 2 and 16, respectively. This explains the significant increase of the scattering rates driven by smaller-scale EHs (especially at low energies). The higher effective frequency v_0 of smaller-scale EHs explains also more efficient scattering of equatorial electrons, $\alpha_0 \sim 90°$, and more efficient momentum scattering (see Figure 10).

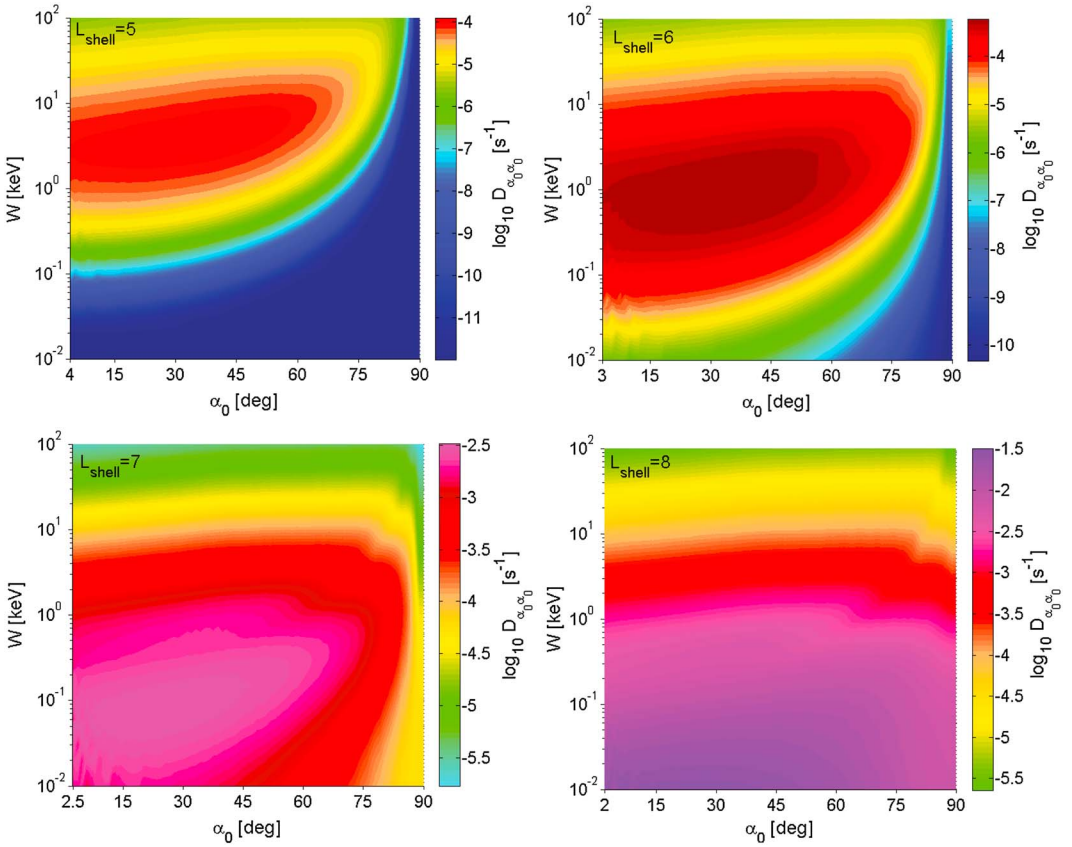


Figure 13. The bounce-averaged pitch angle diffusion coefficients computed for spherical EHs with the velocity $V_\phi = 4000$ km/s and parallel scale $d_\parallel = 0.75$ km at different L shells.

Figure 13 demonstrates pitch angle diffusion coefficients computed for EHs with the moderate parallel scale, $d_{\|} = 0.75$ km, and velocity, $V_{\phi} = 4000$ km/s, at different L shells, $L = 5$, 6, 7, and 8. The most efficient pitch angle scattering at $L = 5$ and $L = 6$ occurs for about 1–6 keV and 0.2–2 keV electrons at rates $D_{\alpha_0\alpha_0} \sim 10^{-4}$ s^{-1} and $D_{\alpha_0\alpha_0} \sim 3 \cdot 10^{-4}$ s^{-1}, respectively. The most efficient pitch angle scattering at $L = 7$ and $L = 8$ occurs for $\lesssim 5$ keV electrons at rates $D_{\alpha_0\alpha_0} \sim 3 \cdot 10^{-3}$ to $3 \cdot 10^{-4}$ s^{-1} and $D_{\alpha_0\alpha_0} \sim 3 \cdot 10^{-2}$ to $3 \cdot 10^{-4}$ s^{-1}, respectively. At higher L shells the most efficient scattering is experienced by lower energy electrons, since the typical energy of gyroresonant electrons $W_0 \propto \omega_0^2 \propto L^{-6}$. The variation of L shell also results in variation of the normalized EH velocity $v_0 \propto \omega_0^{-1} \propto L^3$ and of the multiplicative factor $D_0 \propto \omega_0 W_0^{-2} \propto \omega_0^{-3} \propto L^9$. Both v_0 and D_0 are larger at higher L shells, and this explains the significant increase of the scattering rates at higher L shells and more efficient scattering of equatorial electrons, $\alpha_0 \sim 90°$. In accordance with Figure 10 the momentum scattering is also more efficient at higher L shells. Note that the above estimates implicitly assume that EHs at higher L shells are similar to EHs observed by Van Allen Probes at $L \lesssim 6$.

6. Discussion and Conclusions

The broadband electrostatic wave activity in the Earth plasma sheet was discovered long ago [*Scarf et al.*, 1974; *Gurnett et al.*, 1976], but only the high-cadence electric field measurements on board Geotail showed that this wave activity is due to nonlinear electrostatic solitary waves interpreted as EHs [*Matsumoto et al.*, 1994; *Omura et al.*, 1994]. The modern spacecraft has provided extensive observations of EHs and other solitary waves in the auroral region [*Mozer et al.*, 1997; *Ergun et al.*, 1998a; *Franz et al.*, 2005], in reconnecting current sheets [*Cattell et al.*, 2002; *Matsumoto et al.*, 2003; *Malaspina et al.*, 2013; *Graham et al.*, 2015; *Norgren et al.*, 2015; *Mozer et al.*, 2016b], at collisionless shocks [*Bale et al.*, 1998, 2002; *Williams et al.*, 2005; *Wilson et al.*, 2007; *Hobara et al.*, 2008], and other regions of the near-Earth space (see, e.g., reviews by *Pickett et al.* [2004] and *Mozer et al.* [2015]). Van Allen Probes and THEMIS observations show that EHs and other solitary waves (collectively referred to as TDS) are generated around injection fronts observed in the outer radiation belt [*Mozer et al.*, 2013, 2015; *Malaspina et al.*, 2015] and in the flow braking region [*Deng et al.*, 2010; *Ergun et al.*, 2009, 2015]. *Pickett et al.* [2015] have recently presented observations of TDS in the Saturn radiation belts. Despite extensive observations of TDS in space and laboratory plasmas [*Fox et al.*, 2008, 2012; *Lefebvre et al.*, 2010], their role, to the best of our knowledge, has not been addressed quantitatively. The only exception is likely the paper by *Cranmer and van Ballegooijen* [2003], where it is shown that EHs generated in the extended solar corona due to a turbulence cascade toward electron scales can be responsible for preferential diffusive ion heating in directions transverse to the background magnetic field (for similar effect in the auroral region, see *Ergun et al.* [1998a, 1998b]).

In this paper we have addressed the role of EHs in electron scattering around injection fronts in the outer radiation belt. Since EHs are in principle nonlinear plasma modes [*Gurevich*, 1968; *Schamel*, 1982], the electron scattering rates may not be evaluated via the standard quasi-linear theory [*Vedenov*, 1963; *Drummond and Pines*, 1964; *Kennel and Engelmann*, 1966]. We have obtained analytical formulas describing electron scattering by a single EH and shown that the most efficiently scattered are gyroresonant electrons. The gyroresonance is generally not overlapped with the Landau resonance (for typical EH parameters the overlapping parameter $\Delta_{LC} = \omega_c d_{\|}/\Delta V_L \sim 5 \gg 1$). The partial overlapping of resonances can occur at higher L shells due to lower electron gyrofrequency. Although more detailed analysis of the electron scattering in the regime of partially overlapped resonances, $\Delta_{LC} \sim 1$, should be carried out in the future, the derived analytical formulas provide at least lower estimates of the scattering rates.

We have computed bounce-averaged diffusion coefficients for the prescribed EH spatial distribution and identical parameters for all EHs. We have shown that the diffusion coefficients depend on the EH amplitude Φ_0 and spatial filling factor $n_{\mathrm{EH}} \sim 2/\pi L_{\perp}^2 L_{\|}$ (number of EHs per unit volume) via the multiplicative factor $D_0 \propto \omega_0(\Phi_0/W_0)^2(d_{\|}d_{\perp}^2/L_{\|}L_{\perp}^2)$. We have demonstrated how the normalized diffusion coefficients (diffusion coefficients divided by D_0) depend on the latitudinal extent of EHs and individual EH parameters. The latitudinal extent of EHs influences the scattering rates near the loss cone by a factor of less than 2. Although the latitudinal extent should be carefully addressed in future studies using high-latitude spacecraft observations, its influence on the scattering rates is less significant than the influence of EH parameters (the parallel to transverse scale ratio and normalized velocity). The normalized velocity influences the energy of the most efficiently scattered electrons as well as the scattering rates. In particular, EHs with larger normalized velocities drive more efficient scattering of lower energy electrons, $W \lesssim W_0$. They also provide comparable momentum and pitch angle scattering rates and efficient pitch angle scattering of equatorial electrons, $\alpha_0 \sim 90°$.

We have demonstrated pitch angle scattering rates computed for EHs with the amplitude $\Phi_0 \sim 30$ eV, magnetic field-aligned separation $L_\parallel = 50 d_\parallel$, and minimum possible transverse separation $L_\perp = 5 d_\perp$. The dependence of the diffusion coefficients on individual EH parameters and L shell has been demonstrated. The parameters $(\Phi_0, d_{\parallel,\perp}, V_\phi)$ of EHs observed around injection fronts have actually some occurrence frequency distributions. Moreover, EH parameters can be also related to each other via a nonlinear dispersion relation [*Schamel*, 1982; *Jovanović et al.*, 2002]. The computation of bounce-averaged diffusion coefficients taking into account these factors is left for future studies.

Figures 11–13 show that electrons with energies below about 5 keV can be scattered at rates of about 10^{-2}–10^{-4} s^{-1} corresponding to lifetimes from a few minutes to a few hours (lifetime is estimated as an inverse diffusion coefficient near the loss cone [see, e.g., *Shprits et al.*, 2006]). Therefore, in addition to other wave activities [*Ni et al.*, 2011a, 2011b; *Panov et al.*, 2013], TDS can substantially decrease $\lesssim$5 keV electron fluxes during inward propagation of injection fronts. TDS can provide even the dominant loss mechanism for injections with no significant wave activities at higher frequencies (see, e.g., the injection presented in Figure 1). We point out that TDS can also drive the momentum scattering at rates comparable to the pitch angle scattering. The momentum scattering should be more efficient at higher L shells due to higher EH effective frequency with respect to the electron gyrofrequency. Thus, TDS may be responsible for nonadiabatic heating of electrons below a few keV.

The scattering of $\lesssim$5 keV electrons into the loss cone is responsible for generation of diffuse auroral brightenings [*Swift*, 1981; *Ni et al.*, 2016]. *Thorne* [2010] and *Ni et al.* [2011b] have shown that chorus waves are likely the dominant driver of diffuse aurora precipitations in the outer radiation belt: upper (lower) band chorus waves efficiently scatter $\lesssim$2 keV ($\gtrsim$2 keV) electrons. The typical pitch angle scattering rates are about 10^{-2} s^{-1} for about 1 keV electrons and about 10^{-3} s^{-1} for electrons below and above 1 keV [*Ni et al.*, 2011b]. Electron cyclotron harmonics provide much less efficient scattering in the outer radiation belt [*Ni et al.*, 2008, 2011a] but are believed to be the dominant driver of diffuse aurora precipitations in the outer magnetosphere [*Liang et al.*, 2011; *Ni et al.*, 2012; *Zhang et al.*, 2015]. In the outer radiation belt, electron cyclotron harmonics provide scattering of about 1 keV electrons within a very limited range of pitch angles, $\alpha_0 \lesssim 20°$, at rates 10^{-3}–10^{-4} s^{-1} [*Ni et al.*, 2011b; *Tao et al.*, 2011]. In this paper we have shown that TDS represent an additional potential source for diffuse aurora precipitations. The scattering rates provided by TDS can be comparable to those by chorus waves and may even exceed those for electron cyclotron harmonics. At the same time, realistic occurrence frequency distributions of TDS parameters should be adopted in future studies to compute the diffusion coefficients and clarify the contribution of TDS into intensity of diffuse aurora precipitations in the outer radiation belt.

Appendix A: Calculation of $\Delta W_\perp$

We provide a detailed calculation of the transverse electron energy variation $\Delta W_\perp$ due to a single interaction with EH. The interaction process depends on the distance between EH and electron guiding center, angle ψ setting electron position in the xy plane, and angle φ corresponding to initial electron gyrophase (see Figure 3). In the EH reference frame the unperturbed electron trajectory is a helix:

$$x = \rho \cos\psi - \rho_L \cos(\omega_c t + \psi - \varphi)$$
$$y = \rho \sin\psi - \rho_L \sin(\omega_c t + \psi - \varphi)$$
$$z = (V_\parallel - V_\phi)t\,,$$

where $\rho_L = V_\perp/\omega_c$ is electron gyroradius, $V_\parallel = (2W/m_e)^{1/2}\cos\alpha$ and $V_\perp = (2W/m_e)^{1/2}\sin\alpha$ are unperturbed parallel and transverse velocities, and W and α are electron energy and pitch angle. Performing integration in equation (4) along the unperturbed electron trajectory, we obtain

$$\Delta W_\perp = \Phi_0 \frac{(V_\parallel - V_\phi)^2}{d_\parallel^2} \exp\left[-\frac{\rho^2+\rho_L^2}{2d_\perp^2}\right] \int_{-\infty}^{+\infty} t \exp\left[-\frac{(V_\parallel - V_\phi)^2 t^2}{2d_\parallel^2}\right] \exp\left[\frac{\rho\rho_L}{d_\perp^2}\cos(\omega_c t - \varphi)\right] \mathrm{d}t\,.$$

Making use of the well-known representation [*Morse and Feshbach*, 1953]

$$e^{x\cos\theta} = \sum_{n=-\infty}^{+\infty} I_n(x) e^{-in\theta}\,,$$

where I_n is the nth order modified Bessel function, we find

$$\Delta W_\perp = \Phi_0 \frac{(V_\parallel - V_\phi)^2}{d_\parallel^2} \exp\left[-\frac{\rho^2+\rho_L^2}{2d_\perp^2}\right] \sum_{n=-\infty}^{+\infty} e^{in\varphi} I_n\left(\frac{\rho\rho_L}{d_\perp^2}\right) \int_{-\infty}^{+\infty} t e^{-in\omega_c t} \exp\left[-\frac{(V_\parallel - V_\phi)^2 t^2}{2d_\parallel^2}\right] \mathrm{d}t\,.$$

A straightforward integration results in

$$\Delta W_\perp = -\sqrt{2\pi}\Phi_0 \exp\left[-\frac{\rho^2+\rho_L^2}{2d_\perp^2}\right] \sum_{n=-\infty}^{+\infty} e^{in\varphi} I_n\left(\frac{\rho\rho_L}{d_\perp^2}\right) \frac{i\, n\omega_c d_\parallel}{|V_\parallel - V_\phi|} \exp\left[-\frac{n^2\omega_c^2 d_\parallel^2}{2(V_\parallel - V_\phi)^2}\right]. \quad \text{(A1)}$$

Assuming an ensemble of electrons with uniformly distributed initial gyrophases, we find for ensemble-averaged values $\langle \Delta W_\perp \rangle_\varphi = 0$, while $\langle \Delta W_\perp^2 \rangle_\varphi \neq 0$ and can be written in the form

$$\langle \Delta W_\perp^2 \rangle_\varphi = 4\pi\Phi_0^2 \left(\frac{\omega_c d_\parallel}{V_\parallel - V_\phi}\right)^2 \exp\left[-\frac{\rho^2+\rho_L^2}{d_\perp^2}\right] \sum_{n=1}^{+\infty} n^2 I_n^2\left(\frac{\rho\rho_L}{d_\perp^2}\right) \exp\left[-\frac{n^2\omega_c^2 d_\parallel^2}{(V_\parallel - V_\phi)^2}\right].$$

To clarify the physical sense of the summation in equation (A1), we calculate $\Delta W_\perp$ in a different way. We expand the EH electrostatic potential (1) into the superposition of planar waves, $\Phi(z', r) = (2\pi)^{-3/2} \int \hat{\Phi}(\mathbf{k}) \exp(i\mathbf{k}\mathbf{r}')\mathrm{d}\mathbf{k}$, where $\mathbf{r}' = (x, y, z')$, $\mathbf{k} = \mathbf{k}_\perp + k_\parallel \hat{\mathbf{z}}$ and the spectrum is $\hat{\Phi}(\mathbf{k}) = \Phi_0 d_\parallel d_\perp^2 \exp\left[-(k_\parallel^2 d_\parallel^2 + k_\perp^2 d_\perp^2)/2\right]$. Integrating equation (4) along unperturbed electron trajectories, after some algebra we obtain

$$\Delta W_\perp = -\sqrt{2\pi} \sum_{n=-\infty}^{+\infty} e^{in\varphi} \int_0^{+\infty} \mathrm{d}k_\perp\, k_\perp J_n(k_\perp\rho) J_n(k_\perp\rho_L) \left[i|k_\parallel| \hat{\Phi}(k_\parallel, k_\perp)\right]_{k_\parallel = n\omega_c/(V_\parallel - V_\phi)}. \quad \text{(A2)}$$

The equivalence of equations (A1) and (A2) can be confirmed by taking into account that $\int_0^\infty x e^{-x^2/2} J_n(\alpha x) J_n(\beta x)\mathrm{d}x = e^{-(\alpha^2+\beta^2)/2} I_n(\alpha\beta)$ [*Gradshteyn and Ryzhik*, 1980]. Equation (A2) shows that the scattering is due to electron resonant interaction with electrostatic waves with $k_\parallel = n\omega_c/(V_\parallel - V_\phi)$ and arbitrary n and $k_\perp$. The contribution of each electrostatic wave into the scattering is proportional to electric field amplitude $k_\parallel \hat{\Phi}(k_\parallel, k_\perp)$. Therefore, electrostatic waves interacting with electrons via the Landau resonance have $k_\parallel = 0$ and do not contribute into the scattering. The scattering is entirely due to electrostatic waves interacting with electrons via cyclotron resonances of all orders.

Acknowledgments
All data used in this paper can be found at database (http://www.rbsp-ect.lanl.gov/data-pub/) and at RBSP/EFW database (http://www.space.umn.edu/missions/rbspefw-home-university-of-minnesota/). The work of I.V., O.A., and F.M. was performed under JHU/APL contract 922613 (RBSP-EFW). The work of A.A. was supported by the Russian Foundation for Basic Research grant 15-32-21078. I.V. thanks Ilan Roth for fruitful discussions of the obtained results.

References

Agapitov, O. V., A. V. Artemyev, D. Mourenas, V. Krasnoselskikh, J. Bonnell, O. L. Contel, C. M. Cully, and V. Angelopoulos (2014), The quasi-electrostatic mode of chorus waves and electron nonlinear acceleration, *J. Geophys. Res. Space Physics*, *119*, 1606–1626, doi:10.1002/2013JA019223.

Agapitov, O. V., A. V. Artemyev, D. Mourenas, F. S. Mozer, and V. Krasnoselskikh (2015), Nonlinear local parallel acceleration of electrons through Landau trapping by oblique whistler mode waves in the outer radiation belt, *Geophys. Res. Lett.*, *42*, 10,140–10,149, doi:10.1002/2015GL066887.

Albert, J. M., and S. L. Young (2005), Multidimensional quasi-linear diffusion of radiation belt electrons, *Geophys. Res. Lett.*, *32*, L14110, doi:10.1029/2005GL023191.

Artemyev, A. V., O. V. Agapitov, F. Mozer, and V. Krasnoselskikh (2014), Thermal electron acceleration by localized bursts of electric field in the radiation belts, *Geophys. Res. Lett.*, *41*, 5734–5739, doi:10.1002/2014GL061248.

Bale, S. D., P. J. Kellogg, D. E. Larsen, R. P. Lin, K. Goetz, and R. P. Lepping (1998), Bipolar electrostatic structures in the shock transition region: Evidence of electron phase space holes, *Geophys. Res. Lett.*, *25*, 2929–2932, doi:10.1029/98GL02111.

Bale, S. D., A. Hull, D. E. Larson, R. P. Lin, L. Muschietti, P. J. Kellogg, K. Goetz, and S. J. Monson (2002), Electrostatic turbulence and Debye-scale structures associated with electron thermalization at collisionless shocks, *Astrophys. J.*, *575*, L25–L28, doi:10.1086/342609.

Cattell, C., J. Crumley, J. Dombeck, J. R. Wygant, and F. S. Mozer (2002), Polar observations of solitary waves at the Earth's magnetopause, *Geophys. Res. Lett.*, *29*, 1065, doi:10.1029/2001GL014046.

Cattell, C., et al. (2008), Discovery of very large amplitude whistler-mode waves in Earth's radiation belts, *Geophys. Res. Lett.*, *35*, L01105, doi:10.1029/2007GL032009.

Chandrasekhar, S. (1943), Stochastic problems in physics and astronomy, *Rev. Modern Phys.*, *15*, 1–89, doi:10.1103/RevModPhys.15.1.

Chaston, C. C., et al. (2014), Observations of kinetic scale field line resonances, *Geophys. Res. Lett.*, *41*, 209–215, doi:10.1002/2013GL058507.

Chaston, C. C., J. W. Bonnell, C. A. Kletzing, G. B. Hospodarsky, J. R. Wygant, and C. W. Smith (2015), Broadband low-frequency electromagnetic waves in the inner magnetosphere, *J. Geophys. Res. Space Physics*, *120*, 8603–8615, doi:10.1002/2015JA021690.

Chen, L.-J., J. Pickett, P. Kintner, J. Franz, and D. Gurnett (2005), On the width-amplitude inequality of electron phase space holes, *J. Geophys. Res.*, *110*, A09211, doi:10.1029/2005JA011087.

Cranmer, S. R., and A. A. van Ballegooijen (2003), Alfvénic turbulence in the extended solar corona: Kinetic effects and proton heating, *Astrophys. J.*, *594*, 573–591, doi:10.1086/376777.

Deng, X., M. Ashour-Abdalla, M. Zhou, R. Walker, M. El-Alaoui, V. Angelopoulos, R. E. Ergun, and D. Schriver (2010), Wave and particle characteristics of earthward electron injections associated with dipolarization fronts, *J. Geophys. Res.*, *115*, A09225, doi:10.1029/2009JA015107.

Drummond, W. E., and D. Pines (1964), Nonlinear plasma oscillations, *Ann. Phys.*, *28*, 478–499, doi:10.1016/0003-4916(64)90205-2.

Ergun, R. E., et al. (1998a), FAST satellite observations of large-amplitude solitary structures, *Geophys. Res. Lett.*, *25*, 2041–2044, doi:10.1029/98GL00636.
Ergun, R. E., C. W. Carlson, J. P. McFadden, F. S. Mozer, L. Muschietti, I. Roth, and R. J. Strangeway (1998b), Debye-scale plasma structures associated with magnetic-field-aligned electric fields, *Phys. Rev. Lett.*, *81*, 826–829, doi:10.1103/PhysRevLett.81.826.
Ergun, R. E., C. W. Carlson, L. Muschietti, I. Roth, and J. P. McFadden (1999), Properties of fast solitary structures, *Nonlinear Process. Geophys.*, *6*, 187–194.
Ergun, R. E., et al. (2009), Observations of double layers in Earth's plasma sheet, *Phys. Rev. Lett.*, *102*(15), 155002, doi:10.1103/PhysRevLett.102.155002.
Ergun, R. E., K. A. Goodrich, J. E. Stawarz, L. Andersson, and V. Angelopoulos (2015), Large-amplitude electric fields associated with bursty bulk flow braking in the Earth's plasma sheet, *J. Geophys. Res. Space Physics*, *120*, 1832–1844, doi:10.1002/2014JA020165.
Fox, W., M. Porkolab, J. Egedal, N. Katz, and A. Le (2008), Laboratory observation of electron phase-space holes during magnetic reconnection, *Phys. Rev. Lett.*, *101*(25), 255003, doi:10.1103/PhysRevLett.101.255003.
Fox, W., M. Porkolab, J. Egedal, N. Katz, and A. Le (2012), Observations of electron phase-space holes driven during magnetic reconnection in a laboratory plasma, *Phys. Plasmas*, *19*(3), 32118, doi:10.1063/1.3692224.
Franz, J. R., P. M. Kintner, J. S. Pickett, and L.-J. Chen (2005), Properties of small-amplitude electron phase-space holes observed by Polar, *J. Geophys. Res.*, *110*, A09212, doi:10.1029/2005JA011095.
Glauert, S. A., and R. B. Horne (2005), Calculation of pitch angle and energy diffusion coefficients with the PADIE code, *J. Geophys. Res.*, *110*, A04206, doi:10.1029/2004JA010851.
Glauert, S. A., R. B. Horne, and N. P. Meredith (2014), Three-dimensional electron radiation belt simulations using the BAS Radiation Belt Model with new diffusion models for chorus, plasmaspheric hiss, and lightning-generated whistlers, *J. Geophys. Res. Space Physics*, *119*, 268–289, doi:10.1002/2013JA019281.
Gradshteyn, I. S., and I. M. Ryzhik (1980), *Table of Integrals, Series and Products*, Academic Press, New York.
Graham, D. B., Y. V. Khotyaintsev, A. Vaivads, and M. André (2015), Electrostatic solitary waves with distinct speeds associated with asymmetric reconnection, *Geophys. Res. Lett.*, *42*, 215–224, doi:10.1002/2014GL062538.
Gurevich, A. V. (1968), Distribution of captured particles in a potential well in the absence of collisions, *Soviet J. Exper. Theor. Phys.*, *26*, 575.
Gurnett, D. A., L. A. Frank, and R. P. Lepping (1976), Plasma waves in the distant magnetotail, *J. Geophys. Res.*, *81*, 6059–6071, doi:10.1029/JA081i034p06059.
Hobara, Y., et al. (2008), Cluster observations of electrostatic solitary waves near the Earth's bow shock, *J. Geophys. Res.*, *113*, A05211, doi:10.1029/2007JA012789.
Jovanović, D., P. K. Shukla, L. Stenflo, and F. Pegoraro (2002), Nonlinear model for electron phase-space holes in magnetized space plasmas, *J. Geophys. Res.*, *107*, 1110, doi:10.1029/2001JA900180.
Kellogg, P. J., C. A. Cattell, K. Goetz, S. J. Monson, and L. B. Wilson (2010), Electron trapping and charge transport by large amplitude whistlers, *Geophys. Res. Lett.*, *37*, L20106, doi:10.1029/2010GL044845.
Kennel, C. F., and F. Engelmann (1966), Velocity space diffusion from weak plasma turbulence in a magnetic field, *Phys. Fluids*, *9*, 2377–2388, doi:10.1063/1.1761629.
Kennel, C. F., and H. E. Petschek (1966), Limit on stably trapped particle fluxes, *J. Geophys. Res.*, *71*, 1–28.
Kletzing, C. A., et al. (2013), The Electric and Magnetic Field Instrument Suite and Integrated Science (EMFISIS) on RBSP, *Space Sci. Rev.*, *179*, 127–181, doi:10.1007/s11214-013-9993-6.
Lefebvre, B., L.-J. Chen, W. Gekelman, P. Kintner, J. Pickett, P. Pribyl, S. Vincena, F. Chiang, and J. Judy (2010), Laboratory measurements of electrostatic solitary structures generated by beam injection, *Phys. Rev. Lett.*, *105*(11), 115001, doi:10.1103/PhysRevLett.105.115001.
Liang, J., B. Ni, E. Spanswick, M. Kubyshkina, E. F. Donovan, V. M. Uritsky, R. M. Thorne, and V. Angelopoulos (2011), Fast earthward flows, electron cyclotron harmonic waves, and diffuse auroras: Conjunctive observations and a synthesized scenario, *J. Geophys. Res.*, *116*, A12220, doi:10.1029/2011JA017094.
Liu, J., V. Angelopoulos, X.-J. Zhang, D. L. Turner, C. Gabrielse, A. Runov, J. Li, H. O. Funsten, and H. E. Spence (2016), Dipolarizing flux bundles in the cis-geosynchronous magnetosphere: Relationship between electric fields and energetic particle injections, *J. Geophys. Res. Space Physics*, *121*, 1362–1376, doi:10.1002/2015JA021691.
Lyons, L. R. (1974), General relations for resonant particle diffusion in pitch angle and energy, *J. Plasma Phys.*, *12*, 45–49, doi:10.1017/S0022377800024910.
Lyons, L. R., R. M. Thorne, and C. F. Kennel (1972), Pitch-angle diffusion of radiation belt electrons within the plasmasphere, *J. Geophys. Res.*, *77*, 3455, doi:10.1029/JA077i019p03455.
Ma, Q., D. Mourenas, A. Artemyev, W. Li, R. M. Thorne, and J. Bortnik (2016), Strong enhancement of 10–100 keV electron fluxes by combined effects of chorus waves and time domain structures, *Geophys. Res. Lett.*, *43*, 4683–4690, doi:10.1002/2016GL069125.
Malaspina, D. M., D. L. Newman, L. B. Wilson, K. G. III, P. J. Kellogg, and K. Kersten (2013), Electrostatic solitary waves in the solar wind: Evidence for instability at solar wind current sheets, *J. Geophys. Res. Space Physics*, *118*, 591–599, doi:10.1002/jgra.50102.
Malaspina, D. M., L. Andersson, R. E. Ergun, J. R. Wygant, J. W. Bonnell, C. Kletzing, G. D. Reeves, R. M. Skoug, and B. A. Larsen (2014), Nonlinear electric field structures in the inner magnetosphere, *Geophys. Res. Lett.*, *41*, 5693–5701, doi:10.1002/2014GL061109.
Malaspina, D. M., J. R. Wygant, R. E. Ergun, G. D. Reeves, R. M. Skoug, and B. A. Larsen (2015), Electric field structures and waves at plasma boundaries in the inner magnetosphere, *J. Geophys. Res. Space Physics*, *120*, 4246–4263, doi:10.1002/2015JA021137.
Matsumoto, H., H. Kojima, T. Miyatake, Y. Omura, M. Okada, I. Nagano, and M. Tsutsui (1994), Electrotastic solitary waves (ESW) in the magnetotail: BEN wave forms observed by GEOTAIL, *Geophys. Res. Lett.*, *21*, 2915–2918, doi:10.1029/94GL01284.
Matsumoto, H., X. H. Deng, H. Kojima, and R. R. Anderson (2003), Observation of electrostatic solitary waves associated with reconnection on the dayside magnetopause boundary, *Geophys. Res. Lett.*, *30*, 1326, doi:10.1029/2002GL016319.
Morse, P. M., and H. Feshbach (1953), *Methods of Theoretical Physics*, McGraw-Hill Science/Engineering.
Moya, P. S., V. A. Pinto, A. F. Viñas, D. G. Sibeck, W. S. Kurth, G. B. Hospodarsky, and J. R. Wygant (2015), Weak kinetic Alfvén waves turbulence during the 14 November 2012 geomagnetic storm: Van Allen Probes observations, *J. Geophys. Res. Space Physics*, *120*, 5504–5523, doi:10.1002/2014JA020281.
Mozer, F. S., R. Ergun, M. Temerin, C. Cattell, J. Dombeck, and J. Wygant (1997), New features of time domain electric-field structures in the auroral acceleration region, *Phys. Rev. Lett.*, *79*, 1281–1284, doi:10.1103/PhysRevLett.79.1281.
Mozer, F. S., S. D. Bale, J. W. Bonnell, C. C. Chaston, I. Roth, and J. Wygant (2013), Megavolt parallel potentials arising from double-layer streams in the Earth's outer radiation belt, *Phys. Rev. Lett.*, *111*(23), 235002, doi:10.1103/PhysRevLett.111.235002.
Mozer, F. S., O. Agapitov, V. Krasnoselskikh, S. Lejosne, G. D. Reeves, and I. Roth (2014), Direct observation of radiation-belt electron acceleration from electron-volt energies to megavolts by nonlinear whistlers, *Phys. Rev. Lett.*, *113*(3), 35001, doi:10.1103/PhysRevLett.113.035001.

Mozer, F. S., O. V. Agapitov, A. Artemyev, J. F. Drake, V. Krasnoselskikh, S. Lejosne, and I. Vasko (2015), Time domain structures: What and where they are, what they do, and how they are made, *Geophys. Res. Lett.*, *42*, 3627–3638, doi:10.1002/2015GL063946.

Mozer, F. S., A. Artemyev, O. V. Agapitov, D. Mourenas, and I. Vasko (2016a), Near-relativistic electron acceleration by Landau trapping in time domain structures, *Geophys. Res. Lett.*, *43*, 508–514, doi:10.1002/2015GL067316.

Mozer, F. S., O. A. Agapitov, A. Artemyev, J. L. Burch, R. E. Ergun, B. L. Giles, D. Mourenas, R. B. Torbert, T. D. Phan, and I. Vasko (2016b), Magnetospheric multiscale satellite observations of parallel electron acceleration in magnetic field reconnection by Fermi reflection from time domain structures, *Phys. Rev. Lett.*, *116*(14), 145101, doi:10.1103/PhysRevLett.116.145101.

Muschietti, L., I. Roth, C. W. Carlson, and R. E. Ergun (2000), Transverse instability of magnetized electron holes, *Phys. Rev. Lett.*, *85*, 94–97, doi:10.1103/PhysRevLett.85.94.

Nakamura, R., et al. (2004), Spatial scale of high-speed flows in the plasma sheet observed by Cluster, *Geophys. Res. Lett.*, *31*, L09804, doi:10.1029/2004GL019558.

Newell, P. T., T. Sotirelis, and S. Wing (2009), Diffuse, monoenergetic, and broadband aurora: The global precipitation budget, *J. Geophys. Res.*, *114*, A09207, doi:10.1029/2009JA014326.

Ni, B., R. M. Thorne, Y. Y. Shprits, and J. Bortnik (2008), Resonant scattering of plasma sheet electrons by whistler-mode chorus: Contribution to diffuse auroral precipitation,*Geophys. Res. Lett.*, *35*, L11106, doi:10.1029/2008GL034032.

Ni, B., R. M. Thorne, R. B. Horne, N. P. Meredith, Y. Y. Shprits, L. Chen, and W. Li (2011a), Resonant scattering of plasma sheet electrons leading to diffuse auroral precipitation: 1. Evaluation for electrostatic electron cyclotron harmonic waves, *J. Geophys. Res.*, *116*, A04218, doi:10.1029/2010JA016232.

Ni, B., R. M. Thorne, N. P. Meredith, R. B. Horne, and Y. Y. Shprits (2011b), Resonant scattering of plasma sheet electrons leading to diffuse auroral precipitation: 2. Evaluation for whistler mode chorus waves, *J. Geophys. Res.*, *116*, A04219, doi:10.1029/2010JA016233.

Ni, B., R. M. Thorne, Y. Y. Shprits, K. G. Orlova, and N. P. Meredith (2011c), Chorus-driven resonant scattering of diffuse auroral electrons in nondipolar magnetic fields, *J. Geophys. Res.*, *116*, A06225, doi:10.1029/2011JA016453.

Ni, B., J. Liang, R. M. Thorne, V. Angelopoulos, R. B. Horne, M. Kubyshkina, E. Spanswick, E. F. Donovan, and D. Lummerzheim (2012), Efficient diffuse auroral electron scattering by electrostatic electron cyclotron harmonic waves in the outer magnetosphere: A detailed case study, *J. Geophys. Res.*, *117*, A01218, doi:10.1029/2011JA017095.

Ni, B., R. M. Thorne, X. Zhang, J. Bortnik, Z. Pu, L. Xie, Z.-j. Hu, D. Han, R. Shi, C. Zhou, and X. Gu (2016), Origins of the Earth's diffuse auroral precipitation, *Space Sci. Rev.*, *200*, 205–259, doi:10.1007/s11214-016-0234-7.

Norgren, C., M. André, A. Vaivads, and Y. V. Khotyaintsev (2015), Slow electron phase space holes: Magnetotail observations, *Geophys. Res. Lett.*, *42*, 1654–1661, doi:10.1002/2015GL063218.

Omura, Y., H. Kojima, and H. Matsumoto (1994), Computer simulation of electrostatic solitary waves: A nonlinear model of broadband electrostatic noise, *Geophys. Res. Lett.*, *21*, 2923–2926, doi:10.1029/94GL01605.

Orlova, K. G., and Y. Y. Shprits (2010), Dependence of pitch-angle scattering rates and loss timescales on the magnetic field model, *Geophys. Res. Lett.*, *37*, L05105, doi:10.1029/2009GL041639.

Panov, E. V., A. V. Artemyev, W. Baumjohann, R. Nakamura, and V. Angelopoulos (2013), Transient electron precipitation during oscillatory BBF braking: THEMIS observations and theoretical estimates, *J. Geophys. Res. Space Physics*, *118*, 3065–3076, doi:10.1002/jgra.50203.

Pickett, J., L. Chen, S. Kahler, O. Santolík, D. Gurnett, B. Tsurutani, and A. Balogh (2004), Isolated electrostatic structures observed throughout the Cluster orbit: Relationship to magnetic field strength, *Ann. Geophys.*, *22*, 2515–2523, doi:10.5194/angeo-22-2515-2004.

Pickett, J. S., W. S. Kurth, D. A. Gurnett, R. L. Huff, J. B. Faden, T. F. Averkamp, D. Píša, and G. H. Jones (2015), Electrostatic solitary waves observed at Saturn by Cassini inside 10 R_S and near Enceladus, *J. Geophys. Res. Space Physics*, *120*, 6569–6580, doi:10.1002/2015JA021305.

Reeves, G. D., M. G. Henderson, P. S. McLachlan, R. D. Belian, R. H. W. Friedel, and A. Korth (1996), Radial propagation of substorm injections, in *International Conference on Substorms*, vol. 389, edited by E. J. Rolfe and and B. Kaldeich, p. 579, ESA Special Publication, Paris.

Scarf, F. L., L. A. Frank, K. L. Ackerson, and R. P. Lepping (1974), Plasma wave turbulence at distant crossings of the plasma sheet boundaries and the neutral sheet, *Geophys. Res. Lett.*, *1*, 189–192, doi:10.1029/GL001i005p00189.

Schamel, H. (1982), Kinetic theory of phase space vortices and double layers, *Phys. Scr.*, *2*, 228–237, doi:10.1088/0031-8949/1982/T2A/030.

Sergeev, V. A., V. Angelopoulos, J. T. Gosling, C. A. Cattell, and C. T. Russell (1996), Detection of localized, plasma-depleted flux tubes or bubbles in the midtail plasma sheet, *J. Geophys. Res.*, *101*, 10,817–10,826, doi:10.1029/96JA00460.

Sergeev, V. A., I. A. Chernyaev, S. V. Dubyagin, Y. Miyashita, V. Angelopoulos, P. D. Boakes, R. Nakamura, and M. G. Henderson (2012), Energetic particle injections to geostationary orbit: Relationship to flow bursts and magnetospheric state, *J. Geophys. Res.*, *117*, A10207, doi:10.1029/2012JA017773.

Shklyar, D., and H. Matsumoto (2009), Oblique whistler-mode waves in the inhomogeneous magnetospheric plasma: Resonant interactions with energetic charged particles, *Surv. Geophys.*, *30*, 55–104, doi:10.1007/s10712-009-9061-7.

Shprits, Y. Y., W. Li, and R. M. Thorne (2006), Controlling effect of the pitch angle scattering rates near the edge of the loss cone on electron lifetimes, *J. Geophys. Res.*, *111*, A12206, doi:10.1029/2006JA011758.

Shprits, Y. Y., D. A. Subbotin, N. P. Meredith, and S. R. Elkington (2008), Review of modeling of losses and sources of relativistic electrons in the outer radiation belt II: Local acceleration and loss, *J. Atmos. Sol. Terr. Phys.*, *70*, 1694–1713, doi:10.1016/j.jastp.2008.06.014.

Spence, H. E., et al. (2013), Science goals and overview of the Radiation Belt Storm Probes (RBSP) Energetic Particle, Composition, and Thermal Plasma (ECT) suite on NASA's Van Allen Probes Mission, *Space Sci. Rev.*, *179*, 311–336, doi:10.1007/s11214-013-0007-5.

Su, Z., H. Zheng, and S. Wang (2010), A parametric study on the diffuse auroral precipitation by resonant interaction with whistler mode chorus, *J. Geophys. Res.*, *115*, A05219, doi:10.1029/2009JA014759.

Swift, D. W. (1981), Mechanisms for auroral precipitation—A review, *Rev. Geophys.*, *19*, 185–211, doi:10.1029/RG019i001p00185.

Tao, X., R. M. Thorne, W. Li, B. Ni, N. P. Meredith, and R. B. Horne (2011), Evolution of electron pitch angle distributions following injection from the plasma sheet, *J. Geophys. Res.*, *116*, A04229, doi:10.1029/2010JA016245.

Thorne, R. M. (2010), Radiation belt dynamics: The importance of wave-particle interactions, *Geophys. Res. Lett.*, *37*, L22107, doi:10.1029/2010GL044990.

Thorne, R. M., B. Ni, X. Tao, R. B. Horne, and N. P. Meredith (2010), Scattering by chorus waves as the dominant cause of diffuse auroral precipitation, *Nature*, *467*, 943–946, doi:10.1038/nature09467.

Ukhorskiy, A. Y., and M. I. Sitnov (2013), Dynamics of radiation belt particles, *Space Sci. Rev.*, *179*, 545–578, doi:10.1007/s11214-012-9938-5.

Vasko, I. Y., O. V. Agapitov, F. S. Mozer, and A. V. Artemyev (2015a), Thermal electron acceleration by electric field spikes in the outer radiation belt: Generation of field-aligned pitch angle distributions, *J. Geophys. Res. Space Physics*, *120*, 8616–8632, doi:10.1002/2015JA021644.

Vasko, I. Y., O. V. Agapitov, F. Mozer, A. V. Artemyev, and D. Jovanovic (2015b), Magnetic field depression within electron holes, *Geophys. Res. Lett.*, *42*, 2123–2129, doi:10.1002/2015GL063370.

Vasko, I. Y., O. V. Agapitov, F. S. Mozer, A. V. Artemyev, and J. F. Drake (2016), Electron holes in inhomogeneous magnetic field: Electron heating and electron hole evolution, *Phys. Plasmas*, *23*(5), 52306, doi:10.1063/1.4950834.

Vasko, I. Y., O. V. Agapitov, F. S. Mozer, A. V. Artemyev, J. F. Drake, and I. V. Kuzichev (2017), Electron holes in the outer radiation belt: Characteristics and their role in electron energization, *J. Geophys. Res. Space Physics*, *122*, 120–135, doi:10.1002/2016JA023083.

Vedenov, A. A. (1963), Quasi-linear plasma theory (theory of a weakly turbulent plasma), *J. Nuclear Energy*, *5*, 169–186, doi:10.1088/0368-3281/5/3/305.

Vedenov, A. A., E. P. Velikhov, and R. Z. Sagdeev (1961), Special issue: Stability of plasma, *Soviet Phys. Usp.*, *4*, 332–369, doi:10.1070/PU1961v004n02ABEH003341.

Williams, J. D., L.-J. Chen, W. S. Kurth, D. A. Gurnett, M. K. Dougherty, and A. M. Rymer (2005), Electrostatic solitary structures associated with the November 10, 2003, interplanetary shock at 8.7 AU, *Geophys. Res. Lett.*, *32*, L17103, doi:10.1029/2005GL023079.

Wilson, L. B., III, C. Cattell, P. J. Kellogg, K. Goetz, K. Kersten, L. Hanson, R. MacGregor, and J. C. Kasper (2007), Waves in interplanetary shocks: A Wind/WAVES study, *Phys. Rev. Lett.*, *99*(4), 41101, doi:10.1103/PhysRevLett.99.041101.

Wygant, J. R., et al. (2013), The electric field and waves instruments on the Radiation Belt Storm Probes mission, *Space Sci. Rev.*, *179*, 183–220, doi:10.1007/s11214-013-0013-7.

Xiao, F., Z. Su, H. Zheng, and S. Wang (2009), Modeling of outer radiation belt electrons by multidimensional diffusion process, *J. Geophys. Res.*, *114*, A03201, doi:10.1029/2008JA013580.

Xiao, F., Z. Su, H. Zheng, and S. Wang (2010), Three-dimensional simulations of outer radiation belt electron dynamics including cross-diffusion terms, *J. Geophys. Res.*, *115*, A05216, doi:10.1029/2009JA014541.

Zaslavskii, G. M., and B. V. Chirikov (1971), Stochastic instability of non-linear oscillations, *Sov. Phys. Usp.*, *14*, 549.

Zhang, X.-J., V. Angelopoulos, B. Ni, and R. M. Thorne (2015), Predominance of ECH wave contribution to diffuse aurora in Earth's outer magnetosphere, *J. Geophys. Res. Space Physics*, *120*, 295–309, doi:10.1002/2014JA020455.